Time-Dependent Reliability and Redundancy of Corroded Prestressed Concrete Bridges at Material, Component, and System Levels

Bing Tu[1], You Dong[2*] and Zhi Fang[3]

Abstract:

Due to structural deterioration, performance of concrete bridges degrades with time, which may cause catastrophic failure events, especially for non-redundant structures. This paper develops a methodology for assessing time-variant reliability and redundancy of multi-girder prestressed concrete bridges at material, component, and system levels. Nonlinear analysis is performed to obtain constitutive relationship of reinforced sections and girder components, in which adverse effects of reinforcement corrosion on structural capacity and ductility are considered. Subsequently, the nonlinear finite element analysis is conducted to capture the time-dependent probabilistic resistance of bridge system considering different failure criteria (e.g., serviceability and ultimate limit states). Given the component- and system-level performance indicator, structural capacity-, reliability- and risk-informed redundancy is assessed. The feasibility and capability of proposed approach are illustrated on an existing prestressed concrete bridge. Results demonstrate that the integrated damage mechanism between different levels has a significant effect on the structural ultimate capacity, reliability, and redundancy of corroded structures.

Keywords: System-level performance; Reinforcement corrosion; Ductility; Redundancy; Reliability; Risk; Nonlinear finite element

[1] Assistant Professor, School of Civil Engineering and Architecture, Guangxi University, Nanning, Guangxi 530004, China; formerly, Research Associate, Department of Civil and Environmental Engineering, The Hong Kong Polytechnic University, Hung Hom, Kowloon, Hong Kong, China, tubing2018@gxu.edu.cn.
[2] Assistant Professor of Structural Engineering, Department of Civil and Environmental Engineering, The Hong Kong Polytechnic University, Hung Hom, Kowloon, Hong Kong, China, you.dong@polyu.edu.hk.
[3] Professor, College of Civil Engineering, Hunan University, Changsha, Hunan 410082, China, fangzhi@hnu.edu.cn.
*Corresponding Author.

Introduction

Bridges act as a critical component between communities for transportation of goods and services; and bridge failure could directly affect people's lives. Therefore, safety and performance assessment of bridges receives significant attention. During service life, bridges may be subjected to a variety of stressors, such as aggressive chloride environmental conditions, material aging, and fatigue loading, among others, which could cause a significant reduction of structural performance and even structural failure (Enright and Frangopol 1998; Kassir and Ghosn 2002; Wang *et al.* 2016; Lim et al. 2016; Frangopol et al. 2017; Akiyama *et al.* 2017; Deng *et al.* 2019). Recently, disastrous events, such as collapse of I-35W Mississippi River bridge (Hao 2009), the I-5 Skagit River bridge (Stark et al. 2016), and the Morandi Bridge, have brought new challenges and requirements for assessment and management of aging bridges at both component and system levels. As structures are usually designed to ensure performance and safety at component level, studies on performance of deteriorating bridges at system-level are of vital importance. The system-level reliability and redundancy assessment are conducted in this study to ensure long-term performance of aging bridges at different levels (e.g., material, component, and system).

Structural reliability, accounting for uncertainties of material properties, geometric dimensions, loads, and environmental conditions, is one of the fundamental indicators for performance assessment of bridges (Ditlevsen and Madsen 1996; Thoft-Cristensen and Baker 2012; Sabatino *et al*. 2015; Feng *et al.* 2018; Zheng and Dong 2019). Current design guidelines of bridges are generally established to guarantee a rational reliability index of the load-carrying components (AQSIQ and MOHURD 1999; AASHTO 2007). The component-reliability-oriented design and assessment methodology is

49 associated with several limitations. For instance, load effects of each component are computed using
50 a time-invariant live load distribution factor (LLDF), based on the initial elastic stage (Barr *et al*. 2001;
51 Huo *et al*. 2004; Hughs and Idriss 2006; Yousif and Hindi 2007). Load redistribution among different
52 components within plastic stage is ignored. Additionally, it may neglect the contribution of non-
53 functional transverse connection elements, such as transverse diaphragms and flange wet seams
54 (Eamon and Nowak 2002, 2004). Thus, it is needed to incorporate system reliability with bridge design
55 and assessment process. With respect to system reliability assessment, Estes and Frangopol (1999)
56 developed a series-parallel model for reliability analysis of multi-girder bridges, assuming that failure
57 of any three adjacent girders can cause failure of superstructure system. The proposed model is
58 relatively subjective, and the live load redistribution is not considered. Nowak and Zhou (1990)
59 developed a procedure for resistance and reliability analysis of multi-girder bridges using finite
60 element (FE) modeling. The procedure was adopted within the analysis of several types of bridges,
61 such as steel girder (Czarnecki and Nowak 2008), composite steel girder (Eamon and Nowak 2004;
62 Nowak 2004), reinforced concrete (RC) T-beam (Tabsh and Nowak 1991), and prestressed concrete
63 (PSC) girder (Nowak and Zhou 1990). Though these studies pioneered on the system reliability
64 analysis, more studies should be conducted on the time-dependent reliability incorporating
65 reinforcement corrosion and the effects of structural secondary elements (e.g., diaphragms, barriers)
66 at a multi-scale procedure (e.g., sectional, component, and system).

67 The system redundancy is another essential indicator for system-level structural performance
68 evaluation and for understanding the collapse mechanism of multi-component structures (Ghosn and
69 Moses 1998; Ghosn *et al*. 2010). Redundancy is affected by many factors, such as member behaviour

70 (e.g., ductility, ultimate to yield strength ratio) and configuration characteristics (e.g., member number,
71 connecting strength and stiffness between different members) (Frangopol and Curley 1987). A number
72 of measurements, either deterministic or probabilistic, have been proposed to quantify the redundancy.
73 Most of these quantifications are based on comparisons regarding load-carry capacity or failure
74 probability/reliability indices between intact and damaged system or the most vulnerable component
75 within a system (Moses 1986; Frangopol and Curley 1987; Fu and Frangopol 1990). A risk-informed
76 redundancy/robustness indicator was proposed by Baker *et al*. (2008), in which the probabilities and
77 associated consequences are both considered. Recently, the evolution of system redundancy with time
78 considering structural deterioration effects has attracted research interests. For instance, Okasha and
79 Frangopol (2010) investigated time-variant redundancy of an idealized two parallel bar system
80 subjected to increasing loading and continuous cross-area loss; Saydam and Frangopol (2011)
81 suggested a computational framework for time-variant redundancy index of multi-girder steel bridges;
82 and Biondini and Frangopol (2017) developed a probabilistic procedure for time-dependent
83 redundancy of concrete structures incorporating local damage and ultimate system failure. It should
84 be noted that, corrosion would lead to reduction in strength and transformations of constitutive
85 relationship for reinforcement rebar and prestressed tendons (e.g., from bilinear elastic-plastic to linear
86 elastic) (Barton *et al*. 2000; Darmawan and Stewart 2007; Li *et al*. 2009; Vu *et al*. 2009; Zeng *et al*.
87 2010; Zhang *et al*. 2012; Wang *et al*. 2017), which could affect the girder ductility and system
88 redundancy. However, to the best knowledge of the authors, there are no studies available on the time-
89 dependent redundancy assessment of multi-girder PSC bridges considering the relevant adverse effects
90 induced by corrosion at different levels (e.g., material, section, component, and system) in a

comprehensive manner.

Overall, this paper aims to provide a comprehensive framework to assess structural performance of multi-girder PSC bridges at different levels and analyze the effect of reinforcement corrosion on system performance in terms of reliability and redundancy. A multi-stage nonlinear finite element (FE) analysis-based incremental procedure is proposed to capture the time-dependent structural behavior and system resistance associated with different failure criteria in a life-cycle context. Given the time-dependent probabilistic resistances of individual girder and bridge system associated with both ULS and SLS, the component- and system-level reliability of the bridge can be computed incorporating the probabilistic live load model. Subsequently, by quantifying the differences of nominal resistance, reliability indices, and failure risk between bridge system and the most vulnerable component within the system, the relevant redundancy indicators can be computed. Additionally, an indicator is proposed to quantify the extent of live-load redistribution between different girder components and to enhance the definition of system redundancy. The developed methodology is applied to an existing PSC T-girder bridge.

Time-variant reliability analysis

Limit state function considering corrosion effect

To compute system reliability of a deteriorating bridge, probabilistic models of capacity (resistance) and load effects (demand) at each time point should be established firstly. There are basically two limit states for reinforced and prestressed concrete structures, namely ultimate limit state (*ULS*) and serviceability limit state (*SLS*). *ULS* generally refers to flexural or shear failure of the critical section within a girder component, whereas *SLS* is usually associated with the unacceptable deflection or crack size (Ministry of Transport of the People's Republic of China 2004a). In this paper, resistance of bridge is assessed at both component and system levels considering *ULS* as well as *SLS*. *ULS* and *SLS* of a multi-girder bridge system can be defined as the flexure/shear failure and excessive vertical deflection

115 of the most vulnerable girder within a bridge (Eamon and Nowak 2004), respectively. The system
116 resistance can be defined as the maximum live load (effects) that meets the prescribed limit states. The
117 performance functions of bridge system at time *t*, $G(t)$, can be identified as

118 $$G(t) = R(t) - S(t) \quad (1)$$

119 where $R(t)$ and $S(t)$ = system resistance and live load effects at time *t*, respectively, and both can be
120 expressed in terms of multiples associated with nominal live load model (Frangopol *et al*. 2017). The
121 multiples associated with system resistance refers to the ratio of weight of the maximum live load that
122 induces the predefined limit state (i.e., ULS or SLS) to that of the nominal live load model.

123 Given limit state functions, system reliability index can be computed using First Order Reliability
124 Method (FORM), Second Order Reliability Method (SORM), and Monte Carlo Simulation (MCS)
125 (Ditlevsen and Madsen 1996).

126 **Corrosion model of reinforcement steel**

127 Corrosion of reinforcement steel is one of the primary sources responsible for deterioration of concrete
128 bridges (Enright and Frangopol 1998; Tu *et al*. 2017; Wang *et al*. 2018). Corrosion can introduce
129 section loss, ultimate/yield strength reduction, and stress concentration of reinforcement steel; thus, in
130 turn, this would reduce the structural resistance of individual components as well as the whole system.
131 There are different categories of steel corrosion, among them the most common ones are the
132 carbonization-induced uniform corrosion and pitting corrosion caused by chloride erosion. According
133 to González *et al*. (1995), pitting corrosion results in a much larger penetration depth (e.g., 4 to 8 times)
134 than that of uniform corrosion. Therefore, area loss and decrease of yield/ultimate strength of

135 reinforcement steel under pitting corrosion are accounted for herein. The corrosion initiation time, t_i
136 (years), can be predicted using Fick's law as (Enright and Frangopol 1998)

137 $$t_i = \frac{d^2}{4D_c} \frac{1}{\left[erf^{-1}\left(1 - \frac{C_{cr}}{C_0}\right)\right]^2} \quad (2)$$

138 where d = thickness of concrete cover (cm); D_c = diffusion coefficient of chloride ions (cm^2/year); C_0
139 = constant concentration of chloride ions on concrete surface (% weight of concrete); C_{cr} = threshold
140 value of chloride ions concentration on reinforcement surface (% weight of concrete); and erf^{-1}
141 represents inverse of error function.

142 For normal reinforcement bar, radius of corrosion pit at time t (years), $p(t)$ (mm), can be computed
143 as (Val and Melchers 1997)

144 $$p(t) = 0.0116\left(t - t_i\right) i_{corr} R \quad (3)$$

145 where i_{corr} = corrosion current density ($\mu A/cm^2$) and R = the ratio between maximum and average
146 penetration.

147 Generally, the corrosion in pre-stressing tendons could be induced by inappropriate construction.
148 If pre-stressing tendons are well-installed, corrosion in the tendons is relatively rare. In this paper, in
149 order to illustrate and quantify the potential effects of corrosion on both component- and system-level
150 performance, the deterioration scenario associated with pre-stressing tendons is considered for the
151 investigated PSC bridge.

152 It should be noted that Eq. (2) is suitable for normal reinforcement bars and pre-tensioned tendons
153 that are directly contacted with concrete. For post-tensioned tendon protected by grouted duct, the

corrosion propagation process is much more complicated. With respect to post-tensioned tendon with metal duct, Guo et al. (2016) has developed an approximate procedure for corrosion initiation prediction. Accordingly, the time of corrosion initiation of post-tensioned tendons consists of three parts, namely (1) diffusion time of chloride ions from concrete surface to the metal duct; (2) time for a pit to form on the metallic duct with a depth equal to the thickness of the duct; and (3) diffusion time in grout. The first and third time-counterparts can be computed using Eq. (2), while the second time counterparts can be calculated using Eq. (3) incorporating the duct depth. However, since the duct depth is very thin compared with concrete cover, the second time-counterpart is normally much smaller than the other two time-counterparts. Given more information of the corrosion model associated with post-tensioned tendons, it could be easily updated within the proposed framework for corrosion assessment.

The geometric model proposed by Val and Melchers (1997) can be used to compute loss of effective cross-sectional area under pitting corrosion. Accordingly, net area of reinforcement bar at time t, $A_r(t)$, is (Val and Melchers 1997)

$$A_r(t) = \begin{cases} \dfrac{\pi D_0^2}{4} - A_1 - A_2, & p(t) \le \dfrac{\sqrt{2}}{2} D_0 \\ A_1 - A_2, & \dfrac{\sqrt{2}}{2} D_0 < p(t) \le D_0 \\ 0, & p(t) > D_0 \end{cases} \tag{4}$$

where $\alpha = 2p(t)\sqrt{1-\left[\frac{p(t)}{D_0}\right]^2}$; $\theta_1 = 2\arcsin\left(\frac{\alpha}{D_0}\right)$; $\theta_1 = 2\arcsin\left[\frac{\alpha}{2p(t)}\right]$; $A_1 = \frac{1}{2}\left[\theta_1\left(\frac{D_0}{2}\right)^2 - \alpha\left|\frac{D_0}{2} - \frac{p(t)^2}{D_0}\right|\right]$; $A_2 = \frac{1}{2}\left[\theta_2 p(t)^2 - \alpha\frac{p(t)^2}{D_0}\right]$; and D_0 is the initial diameter of the reinforcement bar.

In addition to the loss of net area, existing laboratory results indicate that corrosion can reduce the yield stress of normal reinforcement bar (Du *et al*. 2005)

$$f_y(t) = \left(1 - 100\alpha_{corr}P_{corr}\right) f_{y0} \tag{5}$$

where $f_y(t)$ = yield stress at time t; f_{y0} = initial yield stress; P_{corr} = percentage of area loss that caused by corrosion (%); and α_{corr} = a coefficient.

With respect to the corrosion of prestressed tendons, the model proposed by Darmawan and Stewart (2007) can be used. Given the corrosion density i_{corr} ($\mu A/\text{cm}^2$), wire length l (mm), and initial corrosion time t_i (years), the probability distribution function (PDF) of $p(t)$ (mm) of single wire is (Darmawan and Stewart 2007)

$$f_{p(t)}\left(t, i_{corr}, l\right) = \frac{\alpha}{\lambda^{0.54}}\exp\left[-\alpha\left(\frac{p(t)}{\lambda^{0.54}} - \mu\right)\right]\exp\left\{-\exp\left[-\alpha\left(\frac{p(t)}{\lambda^{0.54}} - \mu\right)\right]\right\}, t > t_i \tag{6}$$

where

$$\lambda = \frac{D_0^{\,2} - \left[D_0 - 0.0232 i_{corr}\left(t - t_i\right)\right]^2}{D_0^{\,2} - \left(D_0 - 0.0232 i_{corr-\exp} T_{0-\exp}\right)^2} \tag{7}$$

$$\mu = \mu_{0-\exp} + \frac{1}{\alpha_{0-\exp}}\ln\left(\frac{1}{l_{0-\exp}}\right), \quad \alpha = \alpha_{0-\exp} \tag{8}$$

Herein, $T_{0\text{-exp}} = 0.03836$ years, $\mu_{0\text{-exp}} = 0.84$, $\alpha_{0\text{-exp}} = 8.10$, $i_{corr\text{-exp}} = 186\ \mu A/cm^2$, $l_{0\text{-exp}} = 650$ mm, and these values are obtained from statistical analysis of the accelerated corrosion results.

For prestressed strands consisting of seven wires, it is assumed that the pitting only forms on the six outer wires (Darmawan and Stewart 2007). Therefore, the remaining net area of the entire strand $A_{sr}(t)$ is $6A_{wr}(t) + A_{w0}$, where $A_{wr}(t)$ is the remain net area of outer wire at time t, and A_{w0} denotes the time-invariant net area of the inner wire.

Experimental studies show that the ultimate tension strain and stress of prestressed tendons both decrease dramatically with the increase of corrosion extent (Barton *et al*. 2000; Darmawan and Stewart 2007; Li *et al*. 2009; Vu *et al*. 2009; Zeng *et al*. 2010; Zhang *et al*. 2012; Wang *et al*. 2017). In addition, the hardening portion within the constitutive model of prestressed tendons also reduces as the increase of corrosion, which could make the prestressed tendon behave from a bilinear elastic to a brittle elastic (Zeng *et al*. 2010, Wang *et al*. 2017). The evolution of constitutive relationship of corroded prestressed tendon subjected to tension is described by Eqs. (9) and (10) (Zeng *et al*. 2010), as depicted in Fig. 1.

For $P_{corr} \le P_{corr,0}$

$$\sigma_{pc} = \begin{cases} E_{pc}\varepsilon_{pc}; \quad \varepsilon_{pc} \le \dfrac{0.85 f_{puc}}{E_{pc}} \\ 0.85 f_{puc} + \left(\varepsilon_{pc} - \dfrac{0.85 f_{puc}}{E_{pc}}\right)\left(\dfrac{0.15 f_{puc}}{\varepsilon_{puc} - \dfrac{0.85 f_{puc}}{E_{pc}}}\right); \quad \dfrac{0.85 f_{puc}}{E_{pc}} < \varepsilon_{pc} \le \varepsilon_{puc} \end{cases} \tag{9}$$

For $P_{corr} > P_{corr,0}$

$$\sigma_{pc} = E_{pc}\varepsilon_{pc} \tag{10}$$

where $P_{corr,0}$ = threshold value of corrosion extent; σ_{pc} and ε_{pc} = tension stress and strain, respectively; E_{pc}, ε_{puc}, and f_{puc} = elastic modulus, ultimate tension strain, and ultimate tension stress of corroded prestressed tendons, respectively, and can be computed as (Zeng *et al*. 2010)

$$E_{pc} = \left(1 - 0.848 P_{corr}\right) E_p \tag{11}$$

$$\varepsilon_{puc} = \left(1 - 9.387 P_{corr}\right) \varepsilon_{pu} \tag{12}$$

$$f_{puc} = \frac{1 - 2.683 P_{corr}}{1 - P_{corr}} f_{pu} \tag{13}$$

where E_p, ε_{pu}, and f_{pu} = the elastic modulus, ultimate tension strain, and stress of un-corroded prestressed tendons, respectively.

Load model

Bridges are subjected to dead and live loads. Dead load is associated with self-weight of girder, deck, barriers, wearing surface, etc. With respect to live load, the semitrailer truck specified in the Chinese General Code for Design of Highway Bridges and Culverts (Ministry of Transport of the People's Republic of China 2004b) can be selected as the nominal load model. Considering uncertainties of live load, the maximum static live load effect through the lifetime period can be assumed to follow an extreme value distribution (type I) (AQSIQ and MOHURD 1999). Dynamic amplification effect of live load due to deck surface roughness, bridge dynamics, and vehicle dynamics is also considered using a dynamic load amplification factor, η_{DLA} (Ministry of Transport of the People's Republic of China 2004b). Given the load model, the system resistance is expressed in terms of multiples associated with nominal live load model, i.e., ratio between weight of the maximum live load that

induces the predefined limit state (i.e., *ULS* or *SLS*) to that of the nominal live load model. This aspect is discussed in the following section.

System performance considering ductility and redundancy

The system performance is evaluated using FE method in a probabilistic manner. Fig. 2 shows the general procedure for system resistance evaluation considering uncertainties. The detailed information of different modules is indicated in the following sections.

Sectional nonlinear analysis for Moment-Curvature relationship (MCR)

FE method is adopted to compute the resistance of bridge at system level. In order to account for effects of structural ductility and redundancy, material nonlinearity is considered in the FE model. Typically, this can be achieved by introducing the nonlinear constitutive relationships of concrete, reinforcement bar, and prestressed tendons (Guo *et al*. 2010). However, resistance analysis using such an exhaustive model is time-consuming considering numerous elements and incremental analysis procedure (see Fig. 2), not to mention that numerous simulations are required within reliability assessment. Therefore, a simplified and efficient FE methodology, grillage model, is selected for system resistance analysis (Hambly 2014). The grillage method has been demonstrated to have considerable accuracy for girder bridges with simple geometries and load conditions (Jaeger and Bakht 1982; Zokaie *et al*. 1991; Keogh and O'Brien 1996). Additionally, the grillage model has been widely used within the structural resistance analysis process in previous studies (Amer *et al*. 1999; Enright and Frangopol 1999; Al-Saidy *et al*. 2008; Théoret *et al*. 2011; Tu *et al*. 2017). In order to improve the computational efficiency, the grillage model is adopted to compute the probabilistic structural resistance. In grillage models, the

241 RC or PSC girder is modelled by discrete beam elements, for which the constitutive relationship is
242 determined at the sectional level. Therefore, sectional nonlinear analysis should be conducted firstly
243 to obtain sectional constitutive relationship based on the basic material constitutive models. In addition,
244 as the considered limit states of bridge system are associated with flexure failure and excessive
245 deflection, the nonlinear moment-curvature relationship (MCR) is assessed and then introduced into
246 the grillage model.

247 Given geometric sizes and the material constitutive relationships of the PSC section, a numerical
248 incremental algorithm is proposed to determine the MCR, as shown in Fig. 3. With respect to the
249 algorithm, the investigated section is firstly meshed into a number of discrete strips along its height.
250 The initial stress properties as well as the sectional curvature φ_0 of the section caused by prestressed
251 force P_0 is firstly determined based on the on the hypothesis of plane remaining plane and equilibrium
252 regarding axial force. Subsequently, the sectional curvature is increased gradually, and under each
253 given curvature φ_i, based on the hypothesis of plane remaining plane and equilibrium equations
254 regarding axial force, a bisection method-based iterative procedure is conducted to get the critical
255 height of the compression area within the section. Then, the stress properties as well as the integral
256 flexural moment of the section at this stage are obtained. The procedure is terminated when sectional
257 failure happens, corresponding to crushing of concrete at the top fiber or tensile fracture of prestressed
258 tendons. The behavior of concrete under compression is based on the Rusch model (Kupfer *et al.* 1969),
259 in which the ultimate compressive strain is 0.0033 for normal strength concrete. The effects of
260 corrosion on the MCR are considered within the computational process. Based on Eq. (12) the ultimate
261 tension strain of corroded prestressed tendons ε_{puc} is time-dependent and is reduced with time

considering deterioration effects.

Grillage model for resistance analysis

The grillage model, which has been approved to have a good balance between accuracy and computational cost, is adopted herein for assessing the resistance of bridge systems (Hambly 2014). For illustrative purpose, Fig. 4 shows a typical grillage model of a multi-girder bridge. The model consists of five longitudinal members representing the girders. Seven transverse members, labeled as *a*, *b*, *c*, *d*, *e*, *f*, and *g*, represent the transverse diaphragms, which are uniformly distributed along the span. The remaining transverse members are virtual diaphragms, accounting for connection provided by the girder flange. To make it possible to apply load at arbitrary locations in the horizontal plane, shell elements are set upon the longitudinal and transverse beam grid to simulate pressure distribution effect from the deck. The aforementioned nonlinear moment-curvature constitutive relationships are assigned to the longitudinal girder members.

Time-dependent redundancy assessment

Redundancy, a quantitative relationship between component and system safety, is a critical indicator within the performance assessment of structural systems (Ghosn *et al*. 2010; Frangopol *et al*. 2017). Redundancy depends on several factors, for instance, degree of static indeterminacy of the structural system and ductility of the components. For a static determinate system, failure of any component (no matter brittle or ductile) would lead to a structure failure. For a static indeterminate system, the remaining components usually cannot survive once brittle failure of any component happens, as they need to take over the force that is released by the failure component (Frangopol and Curley 1987). In

other words, the component ductility could increase the possibility and extent of force redistribution among components after failure of the weakest component and then contribute the system redundancy (Frangopol and Curley 1987). Therefore, the ductility should be accounted for within the assessment of redundancy.

Generally, ductility is the ability of material, section, component, or system to sustain plastic deformation without significantly reducing its strength (Fajfar 1992). Fig. 5 presents the generalized 'load-to-deformation' relationships associated with different structural constitutes, i.e., ductile material, section, component, and structure, where d_u is the ultimate 'deformation' at failure of ductile material, section, component, and structure system; and d_y is the corresponding 'deformation' at elastic limit. Based on the 'load-to-deformation' relationships, ductility is usually measured using a ductility factor μ, which is the ratio between ultimate 'deformation' at failure d_u to the elastic limit 'deformation' d_y. Obviously, a larger ductility factor indicates a better ductile performance of the investigated structural constitute. Considering the deterioration effects (e.g., steel corrosion), the ductility factors of the structural constitutes should be time-dependent variables.

Different from ductility, redundancy of a structural system is assessed by combing the overall structural performance and its components. Generally, redundancy is defined as the capability of a structure to continue to carry loads after the ductile failure of the most critical component (Hendawi and Frangopol 1994, Ghosn and Moses 1998, Ghosn *et al.* 2010). The conceptual representation for structural behavior of a multi-girder bridge subjected to live load at different time points is shown in Fig. 6. The structural response can be represented by vertical deflection and quantified using the average mid-span displacement of all girders or the maximum displacement among girders. The live

303 load is generalized with respect to the nominal live load model and expressed as a load factor, *LF*. It
304 can be observed that the most vulnerable girder fails (ductile failure) firstly under a load factor of $LF_1(t)$
305 at time *t*, while the bridge system can still sustain extra live load until the ultimate limit state (*ULS*) is
306 approached at $LF_u(t)$, which usually corresponds to the flexural failure of one or several girders that
307 disables the functionality of the bridge system. In addition, there may exists another feature point
308 below $LF_u(t)$ representing another system limit state, e.g., *SLS*, labeled as $LF_s(t)$. It should be noted
309 that the specific structural stages (i.e., $LF_1(t)$, $LF_s(t)$, and $LF_u(t)$) should be characterized based on the
310 structure type, structure configuration, and component behavior, among others. For multi-girder steel
311 and reinforced concrete bridges, ductile failure of the most vulnerable girder generally corresponds to
312 yielding of steel and yielding of rebar within the girder (Hendawi and Frangopol 1994; Ghosn and
313 Moses 1998; Ghosn *et al*. 2010). Therefore, for the investigated PSC bridges in this paper, $LF_1(t)$,
314 $LF_s(t)$, and $LF_u(t)$ refer to the first occurring of yielding, excessive live load deflection (l/100, l is the
315 bridge span), and flexural failure of any girder within the bridge system, respectively. In addition,
316 deterioration effects are considered within the redundancy assessment process.

317 Once the performance curve of the bridge system is obtained, the ratios between the load factor at
318 system limit state ($LF_s(t)$ and $LF_u(t)$) and load factor of the first girder failure ($LF_1(t)$) can be used to
319 quantify the system redundancy, and expressed as (Ghosn and Moses 1998)

320 $$R_u(t) = \frac{LF_u(t)}{LF_1(t)}, \qquad R_s(t) = \frac{LF_s(t)}{LF_1(t)} \tag{14}$$

321 where $R_u(t)$ and $R_s(t)$ = system reserve ratio at time *t* with respect to *ULS* and *SLS*, respectively. Ghosn
322 *et al*. (2010) suggest a minimum value of 1.3 and 1.1 for R_u and R_s to ensure a redundant superstructure

system.

To account for the uncertainties inherent with the structure properties and loads, the difference in reliability index between the system and the most vulnerable girder is used as the probabilistic measure of redundancy (Ghosn and Moses 1998)

$$\Delta\beta_u(t) = \beta_u(t) - \beta_1(t), \qquad \Delta\beta_s(t) = \beta_s(t) - \beta_1(t) \tag{15}$$

where $\Delta\beta_u(t)$ and $\Delta\beta_s(t)$ = probabilistic redundancy measures with respect to *ULS* and *SLS*, respectively; $\beta_u(t)$ and $\beta_s(t)$ = reliability indices of the structure system with respect to *ULS* and *SLS*, respectively; $\beta_1(t)$ = reliability index of the most vulnerable girder and should be computed using $LF_1(t)$ as the capacity. It is suggested that the threshold value of $\Delta\beta_u(t)$ and $\Delta\beta_s(t)$ are 0.85 and 0.25, respectively (Ghosn *et al*. 2010).

To account for the consequences of structural failure, it is necessary to integrate the consequences into the redundancy evaluation. By combining occurrence probabilities of different failure scenarios and corresponding consequences, Baker *et al*. (2008) proposed risk-informed redundancy/robustness measures as

$$R_{r,u}(t) = \frac{R_{Dir}(t)}{R_{Dir}(t) + R_{Idir,u}(t)}, \qquad R_{r,s}(t) = \frac{R_{Dir}(t)}{R_{Dir}(t) + R_{Idir,s}(t)} \tag{16}$$

where $R_{r,u}(t)$ and $R_{r,s}(t)$ = risk-informed redundancy measures with respect to *ULS* and *SLS*, respectively; $R_{Dir}(t)$ = direct risk due to the first girder failure; and $R_{Idir,u}(t)$ and $R_{Idir,s}(t)$ = indirect risk due system failure under *ULS* and *SLS*, respectively. The three risk items involved in Eq. (16) can be computed as

342 $$R_{Dir}(t) = P_{f,1}(t)C_{Dir}(t) \quad (17)$$

343 $$R_{Idir,u}(t) = P_{f,u}(t)C_{Idir,u}(t) \quad (18)$$

344 $$R_{Idir,s}(t) = P_{f,s}(t)C_{Idir,s}(t) \quad (19)$$

345 where $P_{f,1}$, $P_{f,u}$, and $P_{f,s}$ = probabilities of first girder failure, system failure under *ULS* and system
346 failure under *SLS*, respectively; $C_{Dir}(t)$ = direct consequence due to the first girder failure; $C_{Idir,u}(t)$ and
347 $C_{Idir,s}(t)$ = indirect consequences due to system failure under *ULS* and *SLS*, respectively. The direct
348 consequence generally corresponds to potential repair cost of the damaged component. The indirect
349 consequence includes the social and environmental impacts resulting from a failed system (Dong *et al.*
350 2013).

351 The risk-informed redundancy measures defined by Eq. (16) varies between zero and one, and a
352 larger value indicates a smaller ratio between the indirect risk brought by system failure and the direct
353 risk of component failure.

354 **Illustrative example**

355 The proposed methodology is applied to a PSC bridge with a span of 25 *m* as shown in Fig. 7(a). The
356 bridge consists of five 1.4 *m*-height T-shape PSC girders to support a two-lane traffic. The geometric
357 properties and arrangement of reinforcement steel of the girder are presented in Fig. 7(b). Adjacent
358 girders are connected by continuous flange wet seams and seven uniformly-arranged transverse
359 diaphragms (Fig. 7(c)). The bridge was designed based on the Chinese Code for Design of Reinforced
360 Concrete and Prestressed Concrete Highway Bridges and Culverts (Ministry of Transport of the
361 People's Republic of China 2004a). The FE grillage model of investigated bridge is constructed using

362 ANSYS (Ansys 2017).

363 **Component analysis**

364 MCR of the girder (section) is the prerequisites for system resistance analysis and is affected by several
365 parameters. The uncertainties associated with the parameters (e.g., geometric parameters, initial
366 material properties, modeling uncertainty factor, and corrosion-related parameters) are considered
367 within the analysis process, as presented in Table 1.

368 Given the relevant random variables, Latin Hypercube Sampling (LHS), a high-efficiency
369 sampling method (McKay *et al*. 1979), is used to evaluate the statistical properties of MCR of the
370 investigated section (e.g., the mid-span section of each girder) incorporating the incremental numerical
371 algorithm as shown in Fig. 3. At each time step, the time-dependent residual net area and strength of
372 reinforcement steel are computed according to the corrosion model. For instance, given t = 40 years,
373 a portion of the generated MCR curves are shown in Fig. 8(a). It should be noted that moment and
374 curvature presented are the incremental items under external loading, i.e., the initial effects introduced
375 by prestressed tendons are excluded. As indicated, the integral moment of the section increases
376 dramatically with the increase of curvature until prestressed tendons 'yields' (approaches its elastic
377 limit). Afterwards, the sectional moment increases gradually accompanied with a rapid growth of
378 curvature before sectional failure, which corresponds to the crushing of concrete at the top fiber or
379 tensile fracture of prestressed tendons. Therefore, an idealized bilinear model is used to represent the
380 original integral MCRs, as shown in Fig. 8(b), which is characterized by two feature points: yielding
381 point (φ_y, M_y) and failure point (φ_u, M_u).

Distributions of the characteristic parameters of MCR (i.e., M_y, M_u, φ_y and φ_u) at different time points are obtained. To reveal the corrosion effects, expected values of M_y, M_u and φ_y, φ_u as a function of time are shown in Figs. 9(a) and (b), respectively. It can be found that expected values of M_y and M_u both start to decrease at t = 40 years when corrosion of prestressed tendons initiates. The decrease of M_y and M_u is almost synchronous, resulting in a reduction of 15.1% and 13.5% at t = 100 years for M_y and M_u, respectively. The expected value of ultimate curvature (φ_u) also decreases dramatically once the corrosion starts, with a reduction of 47.8% at the end of service time. This is due to the fact that ductility of prestressed tendons reduces dramatically as the corrosion propagates (Zeng *et al*. 2010), making the failure criterion of investigated section transforms from the crushing of top fiber concrete to the tensile fracture of prestressed tendons, while the latter criterion is much more brittle. Comparatively, the expected value of yielding curvature (φ_y) almost keeps constantly within the investigated time interval. The inconsistent deterioration between φ_u and φ_y results in a continuous reduction of sectional ductility. The sectional ductility factor μ_s decreases from 17.8 at t = 0 year to 9.0 at 100 years. Eventually, the moment-curvature slope (i.e., sectional stiffness) of second portion within constitutive model associated with the investigated PSC section (see Fig. 8(b)) increases dramatically under the propagation of steel corrosion.

System resistance and reliability analysis

The system resistance is evaluated using the FE method in a probabilistic manner. Given the associated random variables, the grillage model as indicated in Fig. 4 is implemented with ANSYS to capture the system resistance. Dead load is firstly applied to the FE model, then two side-by-side semitrailer trucks (i.e., the nominal live load model specified in the Chinese General Code for Design of Highway

403 Bridges and Culverts (Ministry of Transport of the People's Republic of China 2004b)) are gradually
404 applied to the model until the predefined limit states are reached. Specifically, the gross vehicle weight
405 (GVW) of the truck is proportionally increased while the distribution factors of per axle are kept
406 constant. The apply locations of the semitrailer trucks are shown in Fig. 4, in which the nominal trucks
407 are also presented. The longitudinal position of the truck load is determined using influence line
408 analysis, and the worst scenario for the flexural moment in mid-span is associated with the case that
409 the front wheel is placed 1.1 m away from the left support. With respect to the transverse direction, the
410 minimum clearance between the two trucks is 1.3 m, and the minimum clearance between the extreme-
411 exterior wheel and the barrier edge is 0.5 m. The system resistance is defined using a load factor, *LF*,
412 which is the ratio between the GVW of the applied live load at failure (i.e., defined limit state) and the
413 GVW of the nominal live load model. A sample of load-deflection curve and load-moment curve at *t*
414 = 40 years are shown in Figs. 10(a) and (b), respectively. The presented vertical deflection and flexural
415 moment are the values of the mid-span section of each girder. As indicated in Figs. 10(a), the load-
416 deflection relationship of individual girder shows obvious nonlinearity under relatively large load due
417 to sectional nonlinearity. The deflection difference among girders is not obvious. This is due to the fact
418 that the wheel loads are nearly uniformly and symmetrically distributed along the bridge deck in
419 transverse direction due to the limited deck width, resulting in that the girders deform nearly parallel
420 in the vertical direction. Fig. 10(b) presents a brief diagram regarding the failure mechanism of the
421 bridge system from component to system level. The flexural moment of all girders increases linearly
422 with the increase of live load at the beginning. Then, girders 3 and 2, which have the lowest yielding
423 strength, yield successively, leading to a decreased moment growth rate of these two girders.

Simultaneously, the other three girders (i.e., girders 1, 4, and 5) take over the loadings released by girders 2 and 3. This is reflected in the load-moment curves through an increased moment-load gradient of these three girders. In the end, the bridge system fails as girder 1 reaches its moment capacity.

Random variables considered in the probabilistic analysis of system resistance include the magnitude of dead load, transverse loading position of live load, and time-dependent characteristic parameters of MCRs (φ_y, φ_u, M_y, and M_u). Herein, dead load is assumed to follow a normal distribution with a bias factor of 1.0148 and a COV of 0.0431 (AQSIQ and MOHURD 1999). The transverse loading position is generated using the probabilistic model proposed by Al-Zaid (1986), in which the distance between the extreme-exterior wheel and the barrier edge (d_1 in Fig. 4) follows a lognormal distribution. The expected values of system resistances as a function of service time are presented in Fig. 11(a) based on the nonlinear finite element modelling. As LF_u and LF_1 are related to the time-dependent ultimate capacity (M_u) and yielding capacity (M_y) of the most critical girder, respectively, the trend of LF_u and LF_1 is in accordance with that of the component resistances (M_u and M_y). Therefore, mean values of LF_u and LF_1 also deteriorate synchronously with time. For instance, the mean value of LF_u and LF_1 at t = 100 years is about 79% and 81% of that at t = 40 years, respectively. Since the criteria of *SLS* is deterministic (l/100) and sectional stiffness of post-yielding stage of the investigated PSC section increases dramatically under the propagation of steel corrosion, the degradation of LF_s due to corrosion is slighter than that of LF_u and LF_1.

Once the time-variant probabilistic models of system resistances are obtained, the corresponding system reliability at each time is calculated using the first order-second moment method (FORM), as shown in Fig. 11(b). The reliability index of the most critical girder component (Girder 1) is also shown

445 in the figure, which is computed using the traditional time-invariant live load distribution factor
446 (LLDF). As indicated, the reliability indices of bridge system are much larger than the reliability index
447 of individual girder, indicating the benefit of redundancy and ductility on structural safety. Specifically,
448 considering corrosion effects, the reliability index of the most critical girder degrades to the threshold
449 (i.e., 4.2) at about 80 years, whereas the two system reliability indices remain above the threshold
450 value through the design service life.

451 **System redundancy analysis**

452 The time-dependent deterministic and probabilistic system redundancy measures (i.e., $R_u(t)$, $R_s(t)$ and
453 $\Delta\beta_u(t)$, $\Delta\beta_s(t)$) are computed using Eqs. (14) and (15), respectively. Fig. 12(a) presents the results of
454 the time-dependent system reserve ratio $R_u(t)$ and $R_s(t)$. As indicated, the system reserve ratios
455 regarding to *ULS* and *SLS* (i.e., $R_u(t)$ and $R_s(t)$) are larger than 1.30 and 1.10 through the service life,
456 indicating a satisfactory redundancy performance. Additionally, considering the load redistribution
457 effects, the value of system reserve ratio under *ULS*, $R_u(t)$, is much larger than the value of component
458 resistance reserve ratio $R_c(t)$ (i.e., $M_u(t)/M_y(t)$).

459 As the system resistance factor associated with *SLS*, LF_s, degrades slighter than LF_1 under
460 corrosion (see Fig. 11(a)), the system reserve ratio associated with *SLS*, $R_s(t)$, increases slightly with
461 time. On the other hand, the system redundancy indicator $R_u(t)$ regarding *ULS* decreases slightly in
462 accordance with the corrosion process (from 1.51 at t = 40 years to 1.46 at t = 100 years), though the
463 component reserve ratio, $R_c(t)$, increases marginally within the time interval. This opposite trend
464 between system reserve ratio $R_u(t)$ and component reserve ratio $R_c(t)$ mainly attributes to the negative
465 effects of corrosion on load redistribution effects at bridge system level. Specifically, as corrosion

466 aggravates, the ductility of girder component μ_c degrades significantly, as shown in Fig. 9(b). While
467 the component ductility is one of the most important preconditions for the occurring of load
468 redistribution among different girders within the bridge system. Therefore, the contribution of
469 component capacity reserve to the system capacity reserve, i.e., system redundancy, is impaired by
470 steel corrosion.

471 To validate the above illustrations regarding the negative effects of steel corrosion on system
472 redundancy, the investigated bridge is re-analyzed by reducing the height of transverse diaphragms
473 from 1.26 *m* to 0.05 *m*. In this way, the transverse connection stiffness of the bridge superstructure as
474 well as the load redistribution effects can be negligible. $R_u(t)$ of the loosened bridge system is shown
475 in Fig. 12(a). As indicated, $R_u(t)$ of the revised bridge system is significantly smaller than that of the
476 original bridge, verifying the fact that transverse diaphragms play an important role within the
477 redundancy of multi-girder bridge. In addition, evolution trend of the updated $R_u(t)$ turns to be
478 consistent with that of the component reserve ratio $R_c(t)$ when the effect of load redistribution is
479 negligible. It should be noted that as the dead load items are extracted within the computation of the
480 load factor LF_u, LF_1 as well as $R_u(t)$, the value of $R_u(t)$ of the loosened bridge is still larger than that of
481 component reserve ratio $R_c(t)$.

482 Considering the importance of load redistribution effect in the mechanism of system redundancy,
483 a new indicator η_{red} is proposed to quantify it and therefore to enhance the definition of redundancy.
484 η_{red} equals to the ratio between system reserve ratio $R_u(t)$ and component reserve ratio $R_c(t)$, as
485 expressed in Eq. (20). Obviously, the value of η_{red} should no less than 1, and a larger value of η_{red}
486 indicates a more profound load redistribution among different components.

$$\eta_{red} = \frac{R_u(t)}{R_c(t)} \tag{20}$$

The time-dependent η_{red} for the initial and loosened bridges are shown in Fig. 12(b). As indicated, the load redistribution indicator η_{red} of the initial bridge system decreases gradually with time due to the component brittleness induced by corrosion (i.e., decrease in component ductility). The values of η_{red} at t = 40 and 100 years are approximate 1.29 and 1.23, respectively. As the load redistribution effect is negligible in the loosened bridge, the redistribution indicator η_{red} of this system fluctuates marginally through the service life. Overall, the formulation mechanism of system redundancy of multi-component structures and the associated effects of steel corrosion can be briefly illustrated in Fig. 13(a).

The probabilistic system redundancy indices $\Delta\beta_u(t)$ and $\Delta\beta_s(t)$ as a function of time are shown in Fig. 13(b). As indicated, the redundancy indices under *ULS* and *SLS* are larger than the threshold value of 0.85 and 0.25 suggested by Ghosn *et. al* (2010). In addition, $\Delta\beta_u(t)$ and $\Delta\beta_s(t)$ gradually decreases and increases with time as the corrosion propagates, respectively, which is similar with $R_u(t)$ and $R_s(t)$. The variation of $\Delta\beta_u(t)$ and $\Delta\beta_s(t)$ is much larger than that of $R_u(t)$ and $R_s(t)$. For instance, the value of $\Delta\beta_u(t)$ at t = 100 years is about 91% of that at t = 40 years, while the reduction of $R_u(t)$ within this time interval is 3%.

The risk-informed redundancy $R_{r,u}$ and $R_{r,s}$ as defined by Eq. (16) is also computed. In the computation, the occurring probabilities associated with different failure scenarios are transformed from the corresponding reliability indices. The consequences of system failure considering *ULS* and *SLS* are assumed to be 100 and 50 times of the consequences of component failure, respectively. It is found that both $R_{r,u}$ and $R_{r,s}$ are varied marginally through the service life of the bridge and almost kept

as 1. This is because the design of the bridge is quite conservative, which is reflected by the relative high reliability indices of both individual girder and the whole system (see Fig. 11(b)).

Conclusions

The paper presents a computational framework for time-dependent system reliability and redundancy assessment of multi-girder PSC bridges. The system-level resistance of the bridge under different failure criteria is evaluated using a multi-stage incremental procedure supported by nonlinear FE method. The effect of reinforcement corrosion on girder capacity and ductility as well as system-level live load redistribution is integrated into the procedure.

The following conclusions are drawn:

(1) At each time step, the moment-curvature relationship (MCR) of the investigated representative PSC section can be idealized by a bilinear model, which could significantly increase the computation efficiency. The expected values of ultimate moment and yielding moment of the section decrease moderately with time. The expected value of ultimate curvature decreases dramatically due to the brittleness brought by corrosion of prestressed tendons, leading to significant reduction in sectional and component ductility.

(2) The reliability indices of bridge system subjected to *ULS* and *SLS* are much larger than the reliability index of individual girder, indicating the benefit of system redundancy and ductility on structural safety. Specifically, considering corrosion effects, the reliability index of single girder degrades to the index threshold (i.e., 4.2) at about 80 years, whereas the two system reliability indices remain above the threshold value through the service life, e.g., 100 years.

(3) The deterministic redundancy regarding *SLS* increases slightly with time as corrosion propagates. In the meantime, since reinforcement corrosion impairs component ductility and then introduces adverse influence on live-load redistribution effect, the system redundancy regarding *ULS* decreases though the component reserve ratio increases marginally through this time interval.

(4) An indicator that equals to the ratio between system reserve ratio and component reserve ratio is proposed to quantify the extent of live-load redistribution between different girder components. It is found that the indicator mainly depends on the stiffness of the structural connection among components (e.g., transverse diaphragms) and structure configurations.

(5) Comparing with the deterministic and risk-informed redundancy measures, the variation of the probabilistic redundancy is much more profound within the service life of the bridge. Therefore, the probabilistic measures may be a better indicator for reflecting the negative effect of reinforcement corrosion on the redundancy property of multi-girder bridges. The propose general framework could also be applied to other types of multi-component structures. The framework can aid in understanding essential parameters as well as formulation mechanism within the computation of system reliability and redundancy, and eventually promote effective and economic design of redundant structure systems in a life-cycle context.

(6) The negative effects of steel corrosion on system reliability and redundancy are emphasized in this paper. The concrete shrinkage, creep and pre-stressing loss could also have some adverse influences on the structural long-term performance. Given more information, these effects can be incorporated within the evaluation process integrating damage mechanism

among different structural levels.

Acknowledgments

The study has been supported by The Hong Kong Polytechnic University under Start-Up Fund number 1-ZE7Q, a grant from the National Natural Science Foundation of China (Grant No. 51808476), and the Project of CNERC fund number 1-BBYU. The opinions and conclusions presented in this paper are those of the authors and do not necessarily reflect the views of the sponsoring organizations.

References

Akiyama, M., Frangopol, D. M., & Takenaka, K. 2017. "Reliability-based durability design and service life assessment of reinforced concrete deck slab of jetty structures." *Structure and Infrastructure Engineering*, 13(4): 468-477.

Al-Saidy, A. H., Klaiber, F. W., Wipf, T. J., Al-Jabri, K. S., and Al-Nuaimi, A. S. 2008. "Parametric study on the behavior of short span composite bridge girders strengthened with carbon fiber reinforced polymer plates." *Constr. Build. Mater.* 22(5): 729-737.

Al-Zaid R. Z. 1986. "Reliability of prestressed concrete girder bridges." PhD dissertation, Univ. of Michigan, Ann Arbor, MI.

Amer, A., Arockiasamy, M., and Shahawy, M. 1999. "Load distribution of existing solid slab bridges based on field tests." *J. Bridge Eng.* 4(3): 189-193.

American Association of State Highway and Transportation Officials (AASHTO). 2007. *LRFD bridge design specifications (4th Edition)*, Washington, D.C.

Ansys. 2017. *Theory reference for ANSYS and ANSYS workbench*, ANSYS, Inc., Southpointe, Canonsburg, PA.

AQSIQ and MOHURD (General Administration of Quality Supervision, Inspection and Quarantine and Ministry of Housing and Urban-Rural Development). 1999. "National standard of the People's Republic of China: Unified standard for reliability design of highway engineering structures." *GB/T 50283-1999*, Beijing (in Chinese).

574 Attard, M. M., and Stewart, M. G. 1998. “A two-parameter stress block for high-strength concrete.”
575 *ACI Struct. J.* 95(3): 305-317.
576 Baker, J. W., Schubert, M., and Faber, M. H. 2008. “On the assessment of robustness.” *Struct. Saf.*
577 30(3): 253-267.
578 Barr, P. J., Eberhard, M. O., and Stanton, J. F. 2001. “Live-load distribution factors in prestressed
579 concrete girder bridges.” *J. Bridge Eng.* 6(5): 298-306.
580 Barton, S. C., Vermaas, G. W., Duby, P. F., West, A. C., and Betti, R. 2000. “Accelerated corrosion and
581 embrittlement of high-strength bridge wire.” *J. Mater. Civ. Eng*. 12(1): 33-38.
582 Biondini, F., and Frangopol, D. M. 2017. “Time-variant redundancy and failure times of deteriorating
583 concrete structures considering multiple limit states.” *Struct. Infrastruct. Eng*. 13(1): 94-106.
584 Czarnecki, A. A., and Nowak, A. S. 2008. “Time-variant reliability profiles for steel girder
585 bridges.” *Struct. Saf.* 30(1): 49-64.
586 Darmawan, M. S., and Stewart, M. G. 2007. “Spatial time-dependent reliability analysis of corroding
587 pretensioned prestressed concrete bridge girders.” *Struct. Saf.* 29(1): 16-31.
588 Deng, L., Yan, W., and Nie, L. 2019. “A simple corrosion fatigue design method for bridges
589 considering the coupled corrosion-overloading effect.” *Eng. Struct*. 178: 309-317. Doi:
590 10.1016/j.engstruct.2018.10.028.
591 Ditlevsen, O., and Madsen, H. O. 1996. *Structural reliability methods*, Wiley, New York.
592 Dong, Y., Frangopol, D. M., and Saydam, D. 2013. “Time- variant sustainability assessment of
593 seismically vulnerable bridges subjected to multiple hazards.” *Earthquake Eng. Struct.*
594 *Dyn.* 42(10): 1451-1467.
595 Du, Y. G., Clark, L. A., and Chan, A. H. C. 2005. “Residual capacity of corroded reinforcing
596 bars.” *Mag. Concrete Res*. 57(3): 135-147.
597 Eamon, C. D., and Nowak, A. S. 2002. “Effects of edge-stiffening elements and diaphragms on bridge
598 resistance and load distribution.” *J. Bridge Eng.* 7(5): 258-266.
599 Eamon, C. D., and Nowak, A. S. 2004. “Effect of secondary elements on bridge structural system
600 reliability considering moment capacity.” *Struct. Saf*. 26(1): 29-47.
601 Enright, M. P., and Frangopol, D. M. 1998. “Probabilistic analysis of resistance degradation of

602 reinforced concrete bridge beams under corrosion." *Eng. Struct*. 20(11): 960-971.
603 Enright, M. P., and Frangopol, D. M. 1999. "Reliability-based condition assessment of deteriorating
604 concrete bridges considering load redistribution." *Struct. Saf.* 21(2): 159-195.
605 Estes, A. C., and Frangopol, D. M. 1999. "Repair optimization of highway bridges using system
606 reliability approach." *J. Struct. Eng.* 125(7): 766-775.
607 Fajfar, P. 1992. "Equivalent ductility factors, taking into account low- cycle fatigue." *Earthquake Eng.*
608 *Struct. Dyn.* 21(10): 837-848.
609 Feng, D., Mauch, C., Summerville, S., and Fernandez, O. 2018. "Suspender Replacement for a
610 Signature Bridge." *Journal of Bridge Engineering*, 23(11): 05018010, 1-10.
611 Frangopol, D. M., and Curley, J. P. 1987. "Effects of damage and redundancy on structural
612 reliability." *J. Struct. Eng.* 113(7): 1533-1549.
613 Frangopol, D. M., Dong, Y., and Sabatino, S. 2017. "Bridge life-cycle performance and cost: analysis,
614 prediction, optimisation and decision-making." *Struct. Infrastruct. Eng*. 13(10): 1-19.
615 Fu, G., and Frangopol, D. M. 1990. "Balancing weight, system reliability and redundancy in a multi-
616 objective optimization framework." *Struct. Saf.* 7(2-4): 165-175.
617 Ghosn, M., and Moses, F. 1998. "Redundancy in highway bridge superstructures." *NCHRP Rep. 406*,
618 Transportation Research Board, Washington, D.C.
619 Ghosn, M., Moses, F., and Frangopol, D. M. 2010. "Redundancy and robustness of highway bridge
620 superstructures and substructures." *Struct. Infrastruct. Eng*. 6(1-2): 257-278.
621 González, J. A., Andrade, C., Alonso, C., and Feliu, S. 1995. "Comparison of rates of general corrosion
622 and maximum pitting penetration on concrete embedded steel reinforcement." *Cem. Concr.*
623 *Res.* 25(2): 257-264.
624 Guo, T., Chen, Z., Liu, T., and Han, D. 2016. "Time-dependent reliability of strengthened PSC box-
625 girder bridge using phased and incremental static analyses." *Eng. Struct*. 117: 358-371.
626 Guo, T., Sause, R., Frangopol, D. M., and Li, A. 2010. "Time-dependent reliability of PSC box-girder
627 bridge considering creep, shrinkage, and corrosion." *J. Bridge Eng.* 16(1): 29-43.
628 Hambly, E. C. 2014. *Bridge deck behavior (2nd Edition)*, Wiley, New York.
629 Hao, S. 2009. "I-35W bridge collapse." *J. Bridge Eng.* 15(5): 608-614.

630 Hendawi, S., and Frangopol, D. M. 1994. “System reliability and redundancy in structural design and
631 evaluation.” *Struct. Saf.* 16(1-2): 47-71.
632 Hughs, E., and Idriss, R. 2006. “Live-load distribution factors for prestressed concrete, spread box-
633 girder bridge.” *J. Bridge Eng.* 11(5): 573-581.
634 Huo, X. S., Wasserman, E. P., and Zhu, P. 2004. “Simplified method of lateral distribution of live load
635 moment.” *J. Bridge Eng.* 9(4): 382-390.
636 Jaeger, L. G., and Bakht, B. 1982. “The grillage analogy in bridge analysis.” *Canadian Journal of Civil*
637 *Engineering*. 9(2): 224-235.
638 Kassir, M. K., and Ghosn, M. 2002. “Chloride-induced corrosion of reinforced concrete bridge decks.”
639 *Cem. Concr. Res.* 32(1): 139-143.
640 Keogh, D.L., and O'Brien, E.J. 1996. “Recommendations on the use of a 3-D grillage model for bridge
641 deck analysis.” *Structural Engineering Review*. 8(4): 357-366.
642 Kupfer H., Hilsdorf H., K., and Rusch H. 1979. “Behavior of concrete under biaxial stresses.” *ACI*
643 *Journal*. 65(8): 656-666.
644 Li, F.M., Yuan, Y. S., Du, J. M., and Ma. H. 2009. “Deterioration of tensile behavior of steel strands
645 corroded by chloride.” *Journal of Southeast University (Natural Science Edition)*. 39(2): 340-344
646 (in Chinese).
647 Li, Y., Bao, W., Guo, X., and Cheng, X. 1997. *Structural reliability and probabilistic limit state design*,
648 China Communications Press, Beijing (in Chinese).
649 Lim, S., Akiyama, M., & Frangopol, D. M. 2016. “Assessment of the structural performance of
650 corrosion-affected RC members based on experimental study and probabilistic modeling.”
651 *Engineering Structures*, 127: 189-205.
652 McKay, M. D., Beckman, R. J., and Conover, W. J. 1979. “Comparison of three methods for selecting
653 values of input variables in the analysis of output from a computer code.” *Technometrics*. 21(2):
654 239-245.
655 Ministry of Transport of the People’s Republic of China. 2004a. “Code for design of highway
656 reinforced concrete and prestressed concrete bridges and culverts.” *JTG D62-2004*, Beijing (in
657 Chinese).

658 Ministry of Transport of the People's Republic of China. 2004b. "General specifications for design of
659 highway bridges and culverts." *JTG D60-2004*, Beijing (in Chinese).
660 Mirza, S. A., MacGregor, J. G., and Hatzinikolas, M. 1979. "Statistical descriptions of strength of
661 concrete." *J. Struct. Div. ASCE.* 105(6): 1021-1037.
662 Moses, F. 1986. "Optimum design, redundancy and reliability of structural systems." *Comput.*
663 *Struct.* 24(2): 239-251.
664 Nowak, A. S. 2004. "System reliability models for bridge structures." *Bulletin of the Polish Academy*
665 *of Sciences Technical Sciences*. 52(4): 321-328.
666 Nowak, A. S., and Zhou, J. 1990. "System reliability models for bridges." *Struct. Saf.* 7(2-4): 247-254.
667 Okasha, N. M., and Frangopol, D. M. 2010. "Time-variant redundancy of structural systems." *Struct.*
668 *Infrastruct. Eng*. 6(1-2): 279-301.
669 Sabatino, S., Frangopol, D.M., and Dong, Y. 2015. "Sustainability-informed maintenance optimization
670 of highway bridges considering multi-attribute utility and risk attitude." *Eng. Struct*. 102: 310-
671 321.
672 Saydam, D., and Frangopol, D. M. 2011. "Time-dependent performance indicators of damaged bridge
673 superstructures." *Eng. Struct*. 33(9): 2458-2471.
674 Stark, T. D., Benekohal, R., Fahnestock, L. A., LaFave, J. M., He, J., and Wittenkeller, C. 2016. "I-5
675 Skagit River Bridge Collapse Review." *J. Perform. Constr. Facil*. 30(6): 04016061.
676 Stewart, M. G., and Rosowsky, D. V. 1998. "Time-dependent reliability of deteriorating reinforced
677 concrete bridge decks." *Struct. Saf.* 20(1): 91-109.
678 Tabsh, S. W., and Nowak, A. S. 1991. "Reliability of highway girder bridges." *J. Struct. Eng.* 117(8):
679 2372-2388.
680 Théoret, P., Massicotte, B., and Conciatori, D. 2011. "Analysis and design of straight and skewed slab
681 bridges." *J. Bridge Eng*. 17(2): 289-301.
682 Thoft-Cristensen, P., and Baker, M. J. 2012. *Structural reliability theory and its applications*, Springer,
683 New York.
684 Tu, B., Fang, Z., Dong, Y., and Frangopol, D. M. 2017. "Time-variant reliability analysis of widened
685 deteriorating prestressed concrete bridges considering shrinkage and creep." *Eng. Struct*. 153: 1-

16.

Val, D. V., and Melchers, R. E. 1997. "Reliability of deteriorating RC slab bridges." *J. Struct. Eng.* 123(12): 1638-1644.

Val, D. V., and Trapper, P. A. 2008. "Probabilistic evaluation of initiation time of chloride-induced corrosion." *Reliab. Eng. Syst. Saf.* 93(3): 364-372.

Vu, N. A., Castel, A., and François, R. 2009. "Effect of stress corrosion cracking on stress–strain response of steel wires used in prestressed concrete beams." *Corros. Sci.* 51(6): 1453-1459.

Wang, L., She, Q., Zhang, X. H., and Zhang, J. R. 2017. "Study of Mechanical Property of Prestressed Strands Corroded in Artificial Climate." *Journal of Highway and Transportation Research and Development*. 34(1): 97-102 (in Chinese).

Wang, W., Deng, L. and Shao, X. 2016. "Number of Stress Cycles for Fatigue Design of Simply-Supported Steel I-girder Bridges Considering the Dynamic Effect of Vehicle Loading." *Eng. Struct*. 110: 70-78.

Wang, Z., Jin, W., Dong, Y., and Frangopol, D.M. 2018. "Hierarchical life-cycle design of reinforced concrete structures incorporating durability, economic efficiency and green objectives." *Eng. Struct*. 157: 119-131.

Yousif, Z., and Hindi, R. 2007. "AASHTO-LRFD live load distribution for beam-and-slab bridges: Limitations and applicability." *J. Bridge Eng.* 12(6): 765-773.

Zeng, Y. H., Gu, X. L., Zhang, W. P., and Huang, Q. H. 2010. "Study on mechanical properties of corroded prestressed tendons." *Journal of Building Materials*. 13(2): 169-174 (in Chinese).

Zhang, W., Song, X., Gu, X., and Li, S. 2012. "Tensile and fatigue behavior of corroded rebars." *Constr. Build. Mater.* 34: 409-417.

Zheng, Y., and Dong, Y. 2019. "Performance-based assessment of bridges with steel-SMA reinforced piers in a life-cycle context by numerical approach." *Bulletin of Earthquake Engineering* 17(3): 1667-1688.

Zokaie, T., Osterkamp, T. A., and Imbsen, R. A. 1991. "Distribution of Wheel Loads on Highway Bridges." *NCHRP Proj. Rep. 12-26*, Transportation Research Board, Washington, D.C.

List of Tables

Table 1. Random variables involved in component analysis

Variable	Properties	Mean	COV	Distribution type	References
b'_f	Effective width of flange	1.0013[a]	0.0081	Normal	AQSIQ and MOHURD 1999
b	Width of web	1.032[a]	0.1019	Normal	AQSIQ and MOHURD 1999
h'_f	Height of flange	1.032[a]	0.1019	Normal	AQSIQ and MOHURD 1999
h_0	Effective height of section	1.0124[a]	0.0229	Normal	AQSIQ and MOHURD 1999
a'_s	Distance from the top fiber to the centroid of the compressive reinforcement	1.0178[a]	0.0496	Normal	AQSIQ and MOHURD 1999
h	Nominal height of the section	1.032[a]	0.1019	Normal	AQSIQ and MOHURD 1999
d	Thickness of concrete cover	1.0178[a]	0.0496	Normal	AQSIQ and MOHURD 1999
A_s, A'_s, A_p	Initial area of tensile reinforcement, compressive reinforcement and prestressed tendon	1.000[a]	0.0350	Normal	AQSIQ and MOHURD 1999
f_c (MPa)	Compressive strength of concrete	39.9	0.15	Lognormal	Attard and Stewart 1998
f_{y0} (MPa)	Initial yield strength of reinforcement bar	369	0.0719	Normal	AQSIQ and MOHURD 1999, Ministry of Transport of the People's Republic of China 2004a
f_{pu} (MPa)	Initial ultimate strength of prestressed tendons	1932	0.0142	Normal	Mirza *et al*. 1979
k_{pM}	Modeling uncertainty factor for flexural moment capacity	1.110	0.062	Normal	Li *et al*. 1997
D_c (cm^2/year)	Diffusion coefficient	0.631	0.2	Lognormal	Val and Trapper 2008
C_0 (kg/m^3)	Surface chloride content	15	0.2	Normal	Val and Trapper 2008
C_{cr} (kg/m^3)	Threshold chloride concentration	2.0	0.2	Normal	Val and Trapper 2008
i_{corr} ($\mu A/cm^2$)	Corrosion current density	1.0	0.2	Normal	González *et al*. 1995
R	Penetration ratio	3.0	0.33	Normal	Stewart and Rosowsky 1998

Note: [a]The normalized value divided by nominal value.

Figure 1

Click here to access/download;Figure;Fig 1.pdf

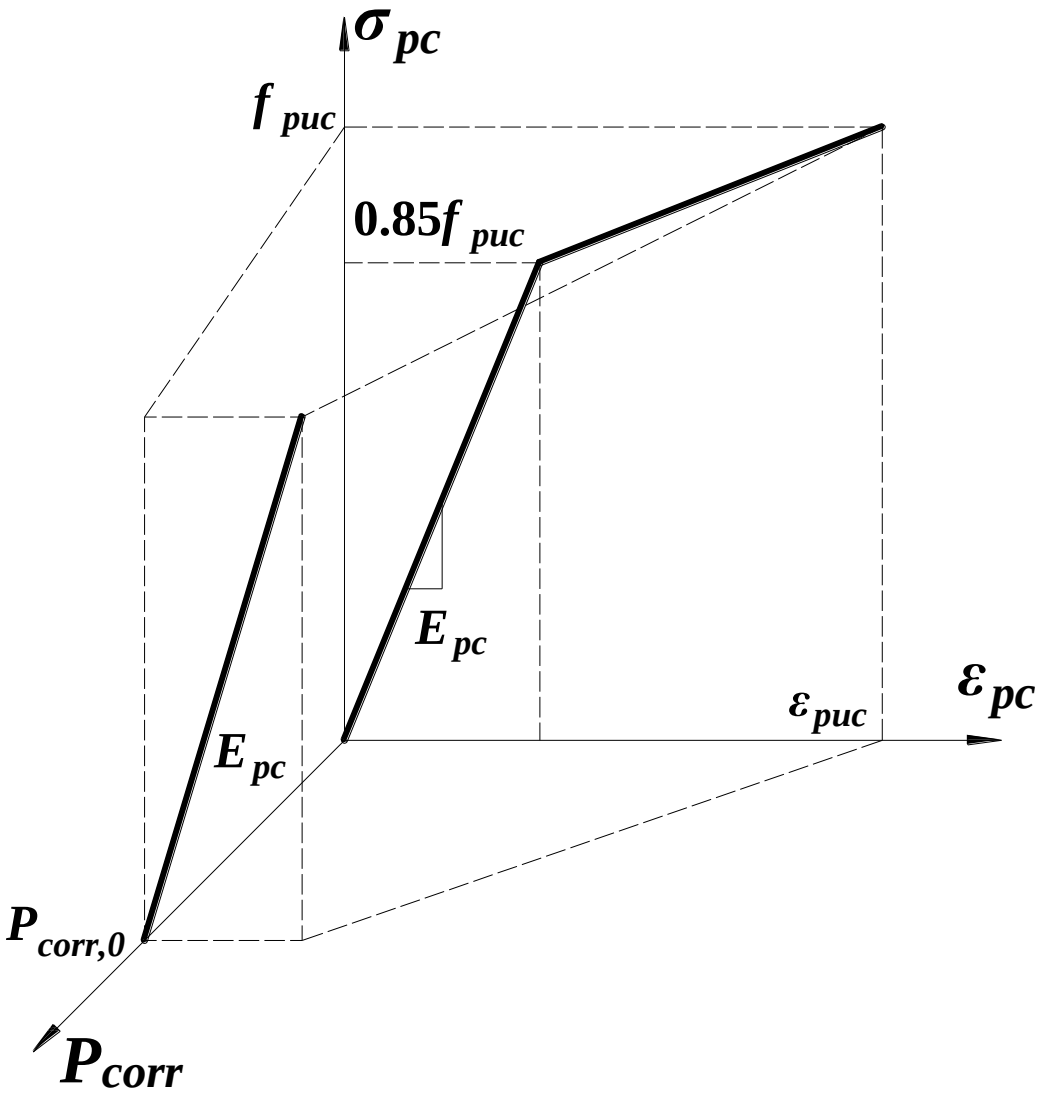

Figure 2

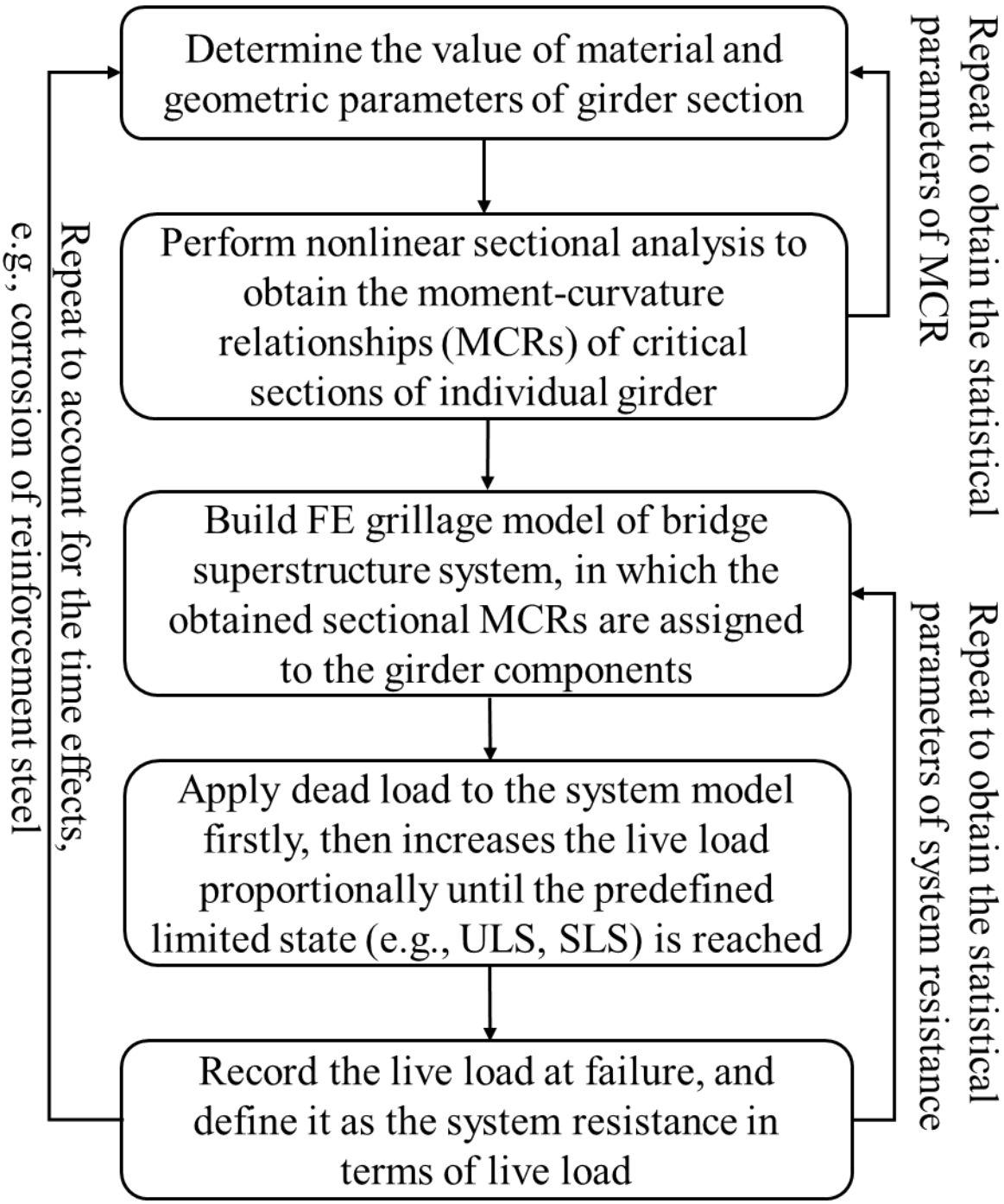

Figure 3 Click here to access/download;Figure;Fig 3.pdf

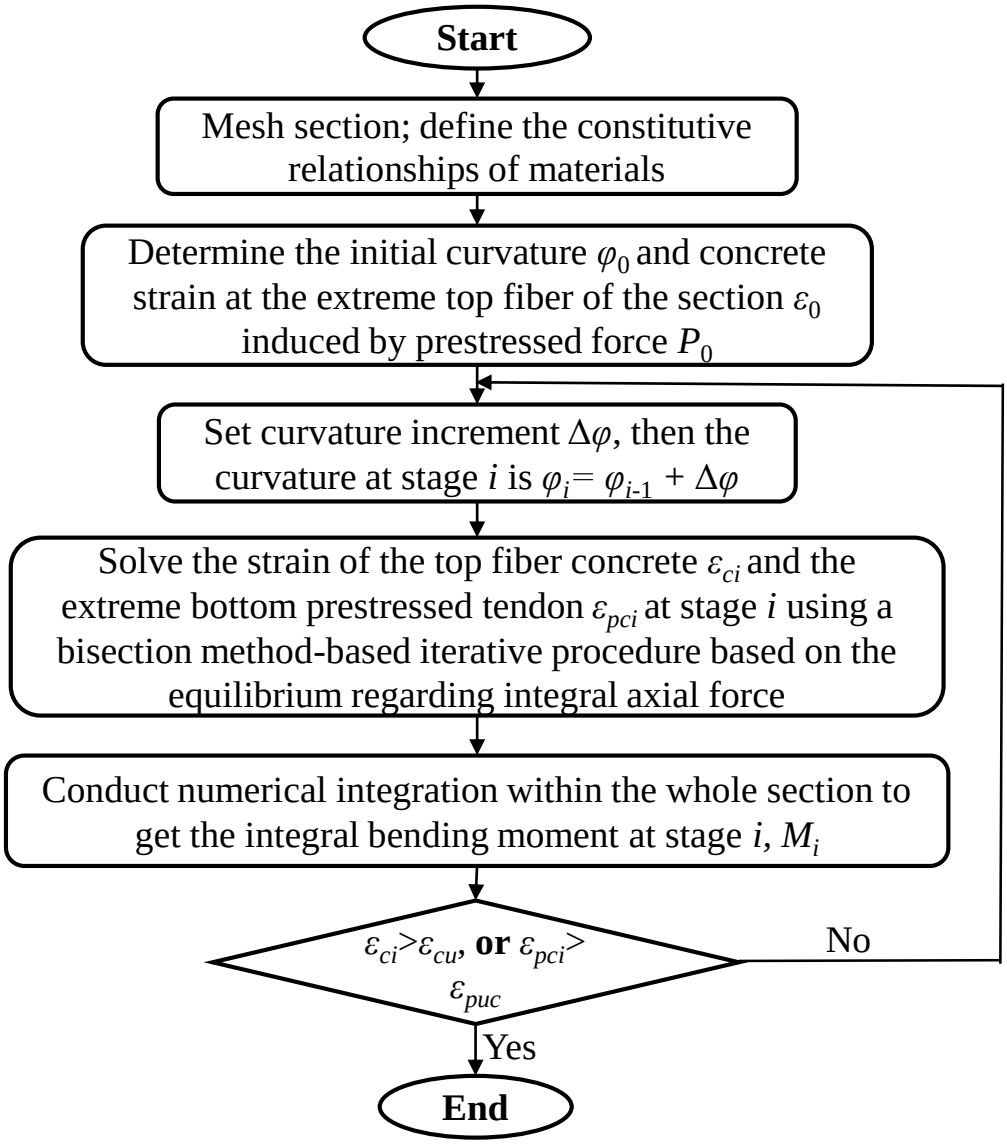

Figure 4

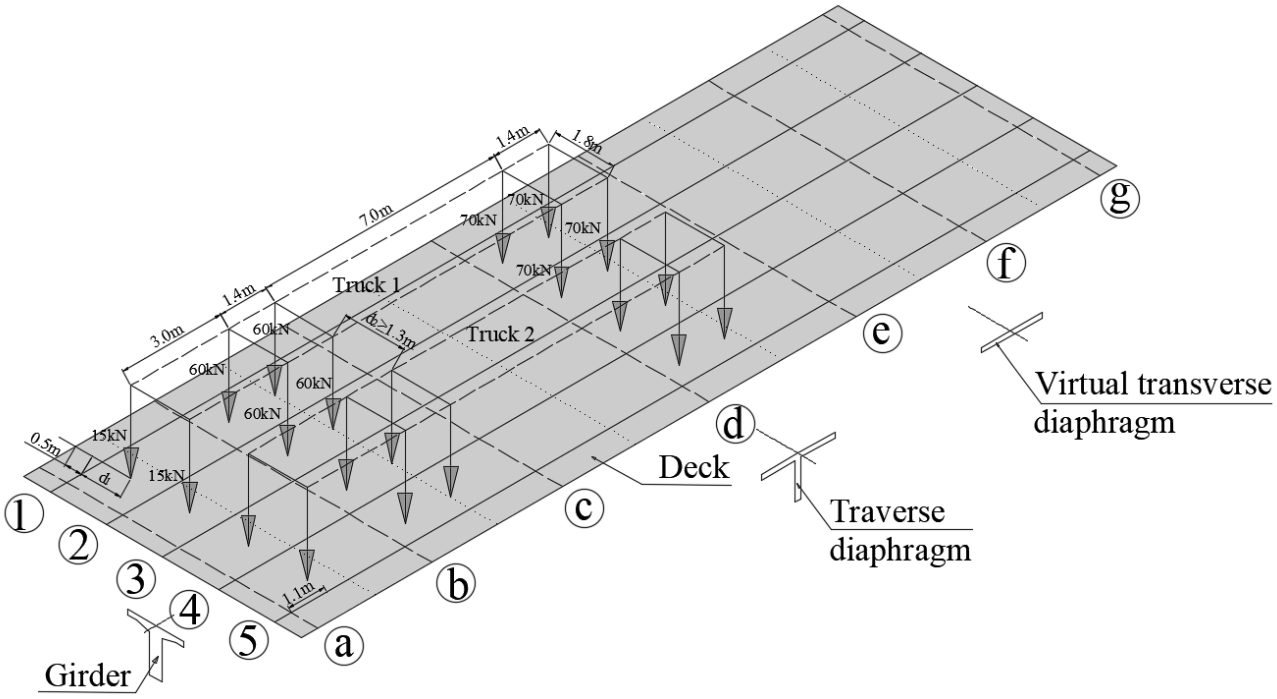

Figure 5

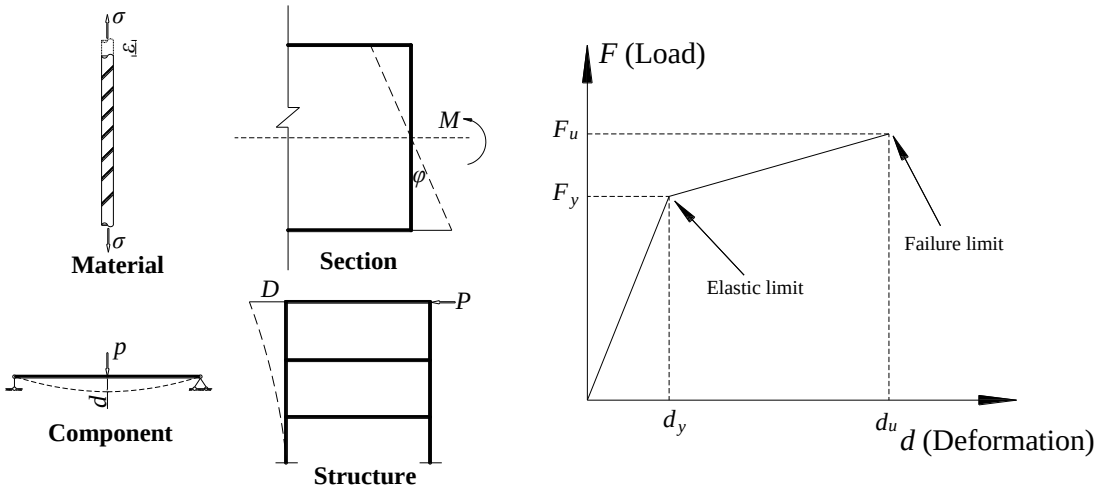

Figure 6

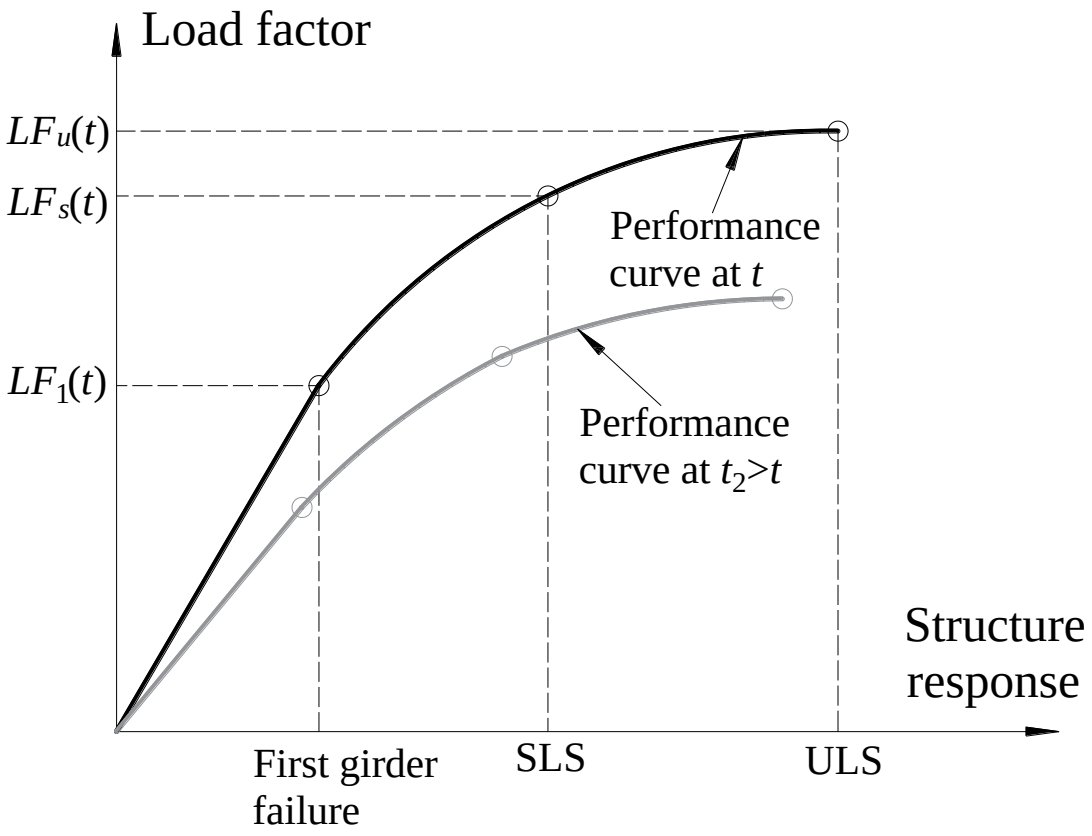

Figure 7 Click here to access/download;Figure;Fig 7.pdf

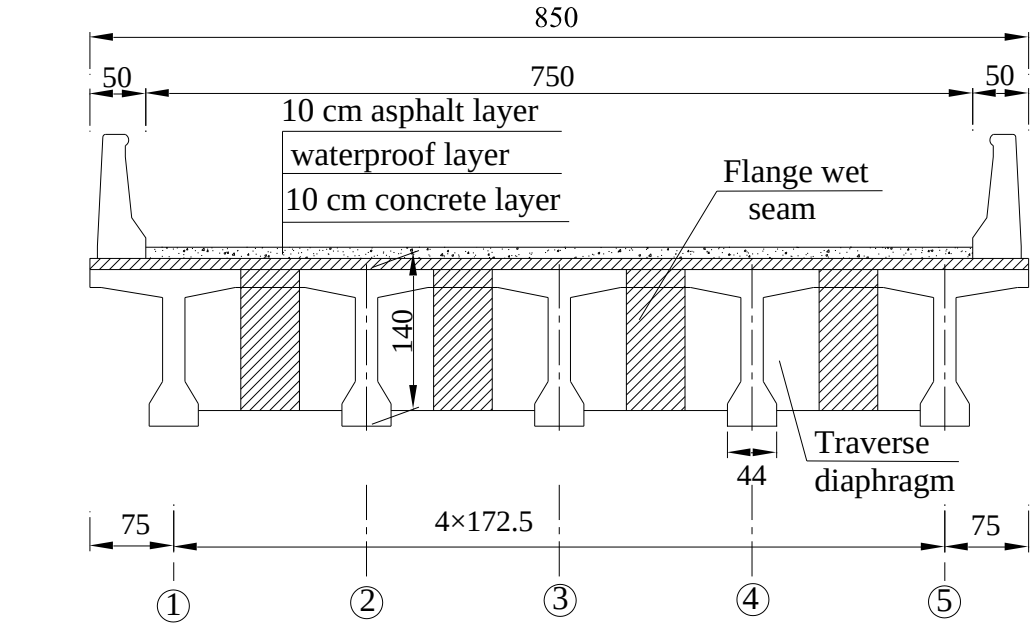

(a)

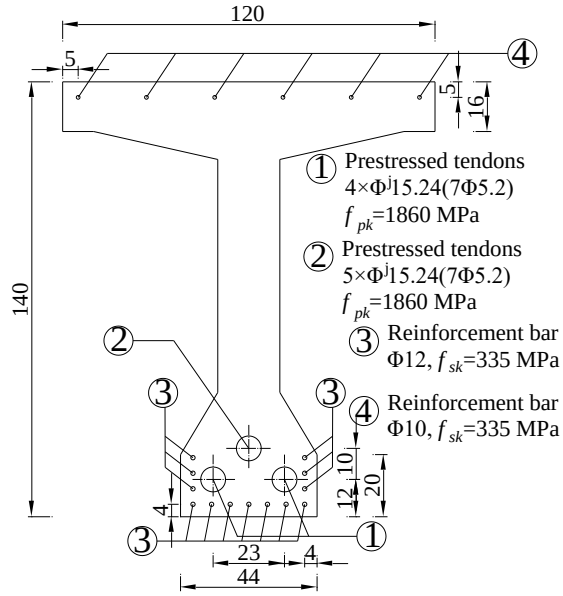

(b)

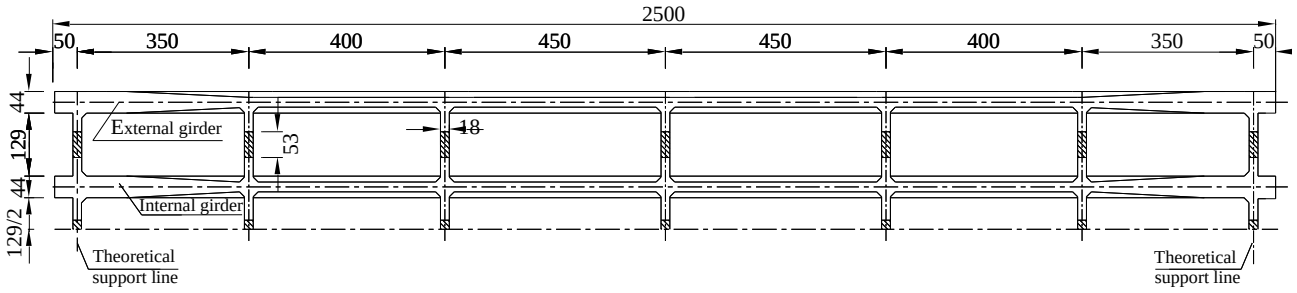

(c)

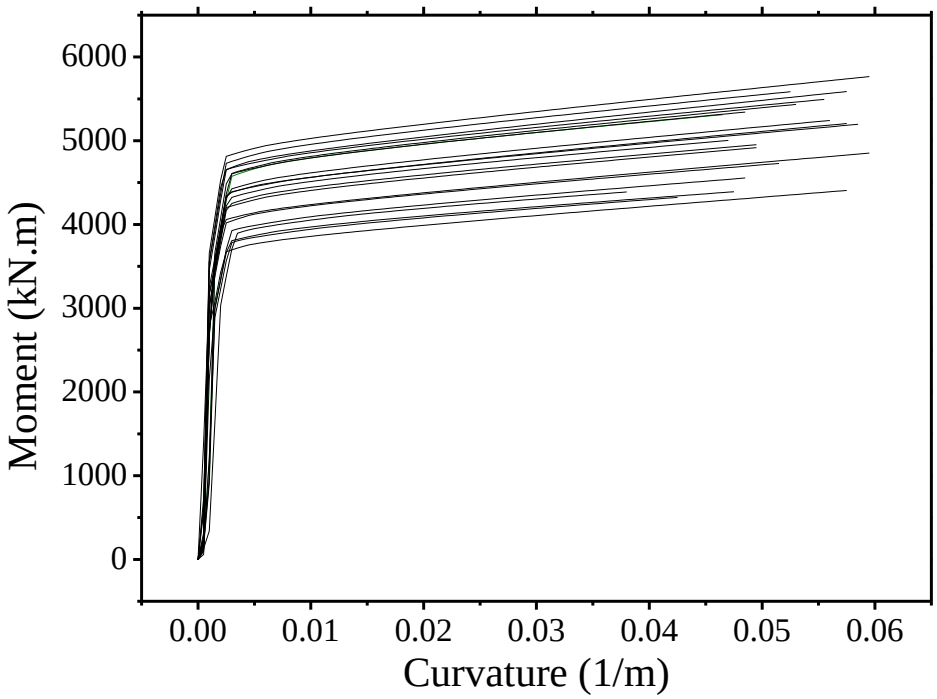

(a)

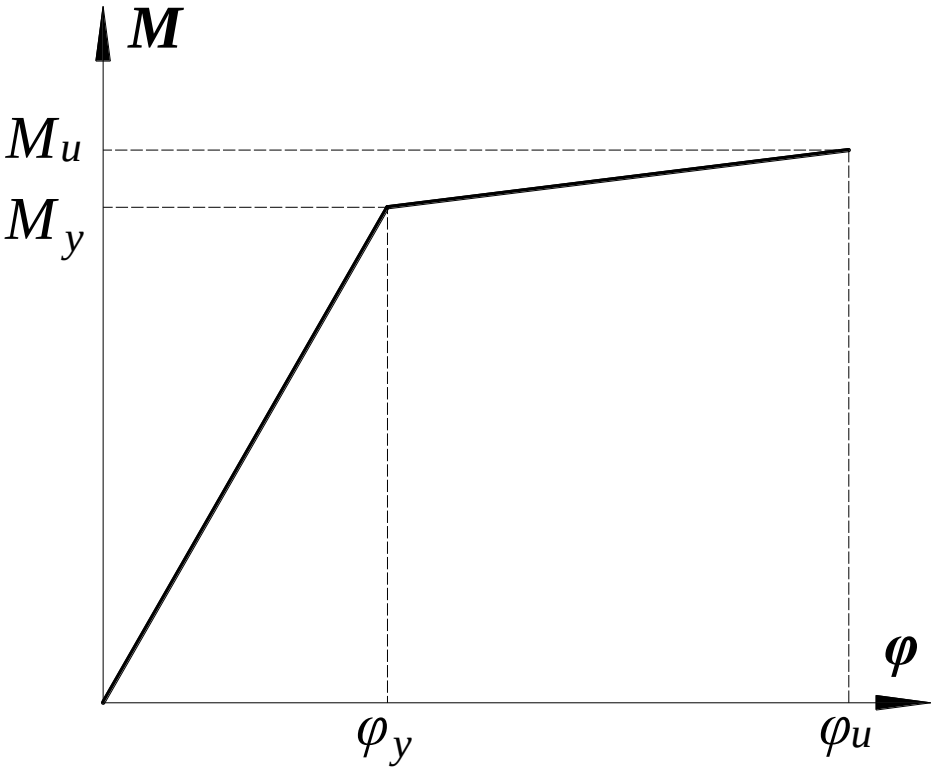

(b)

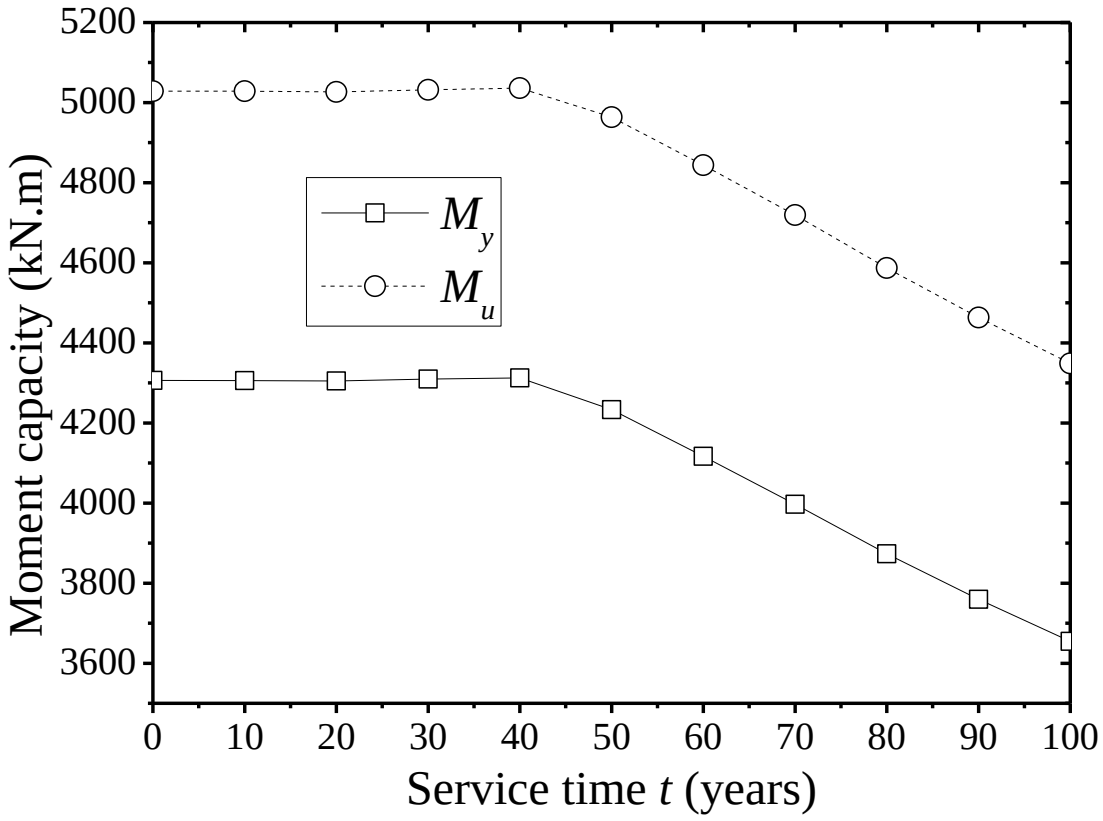

(a)

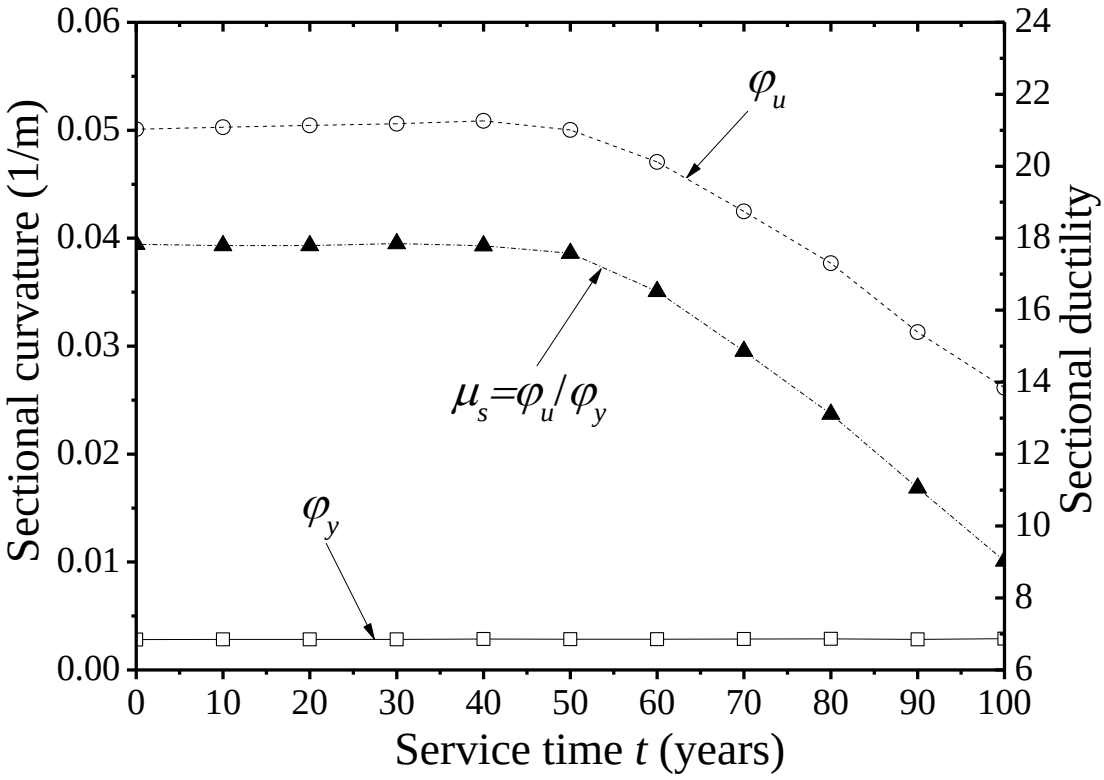

(b)

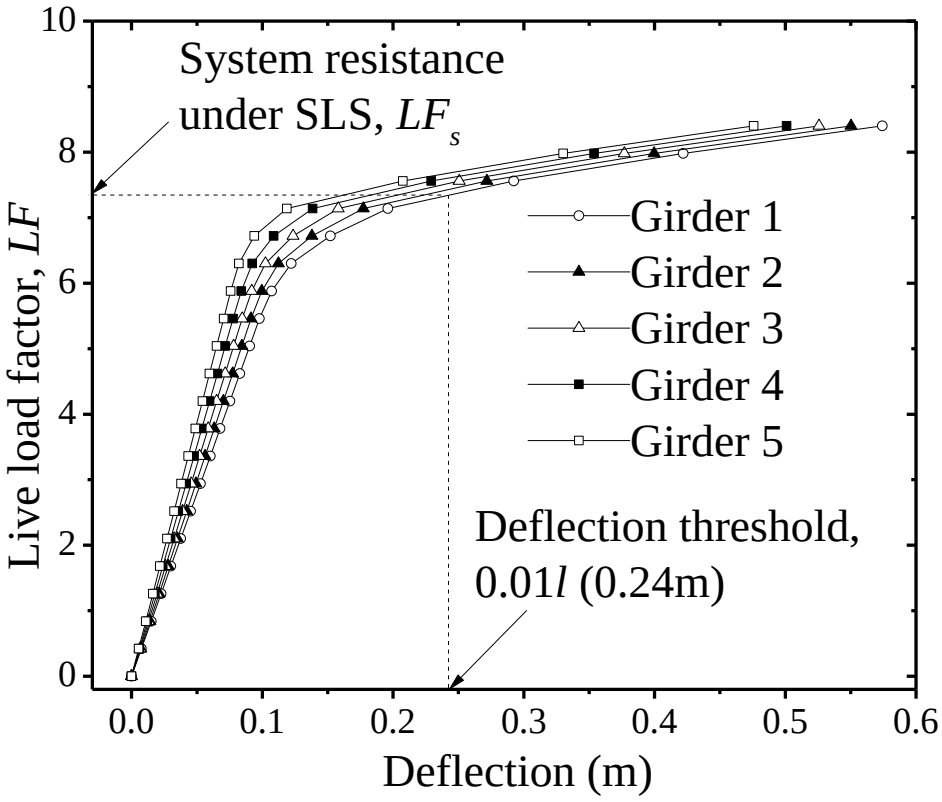

(a)

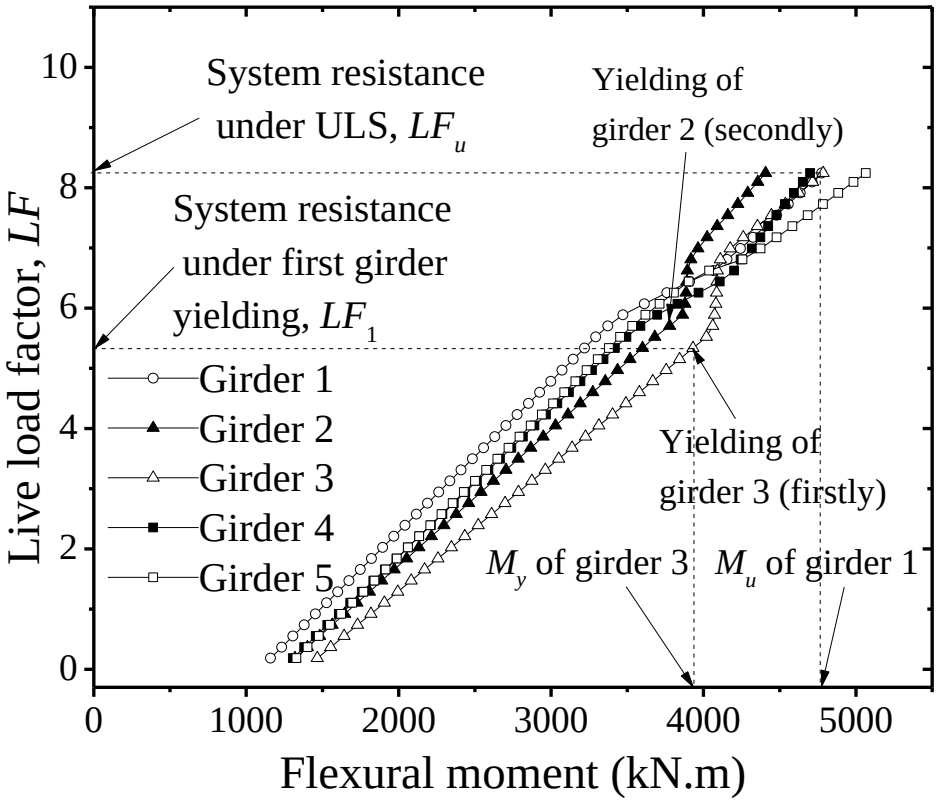

(b)

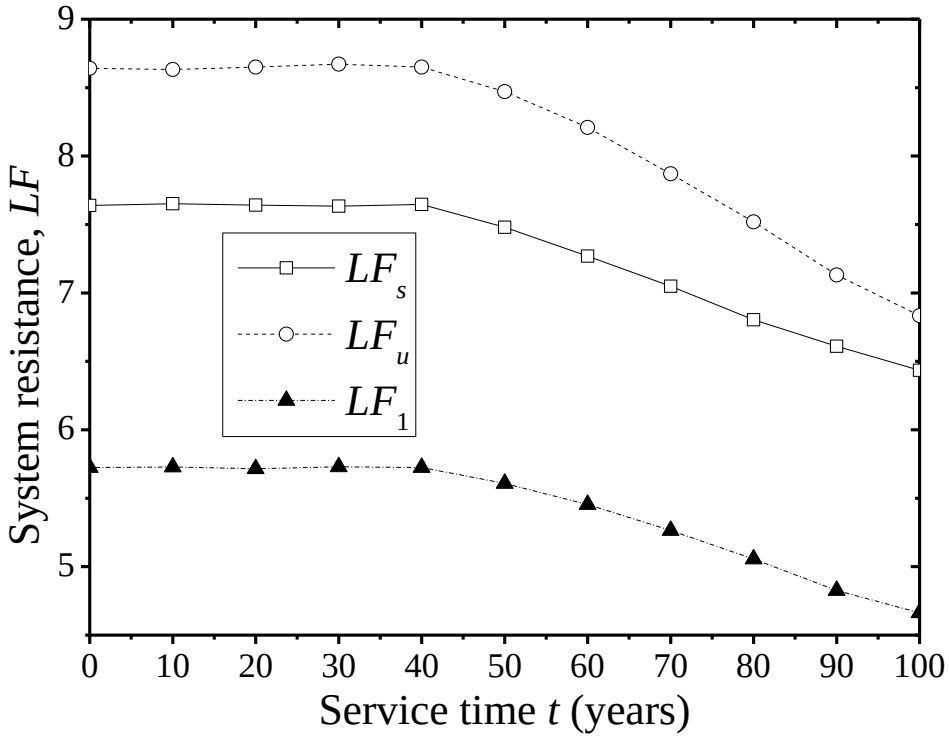

(a)

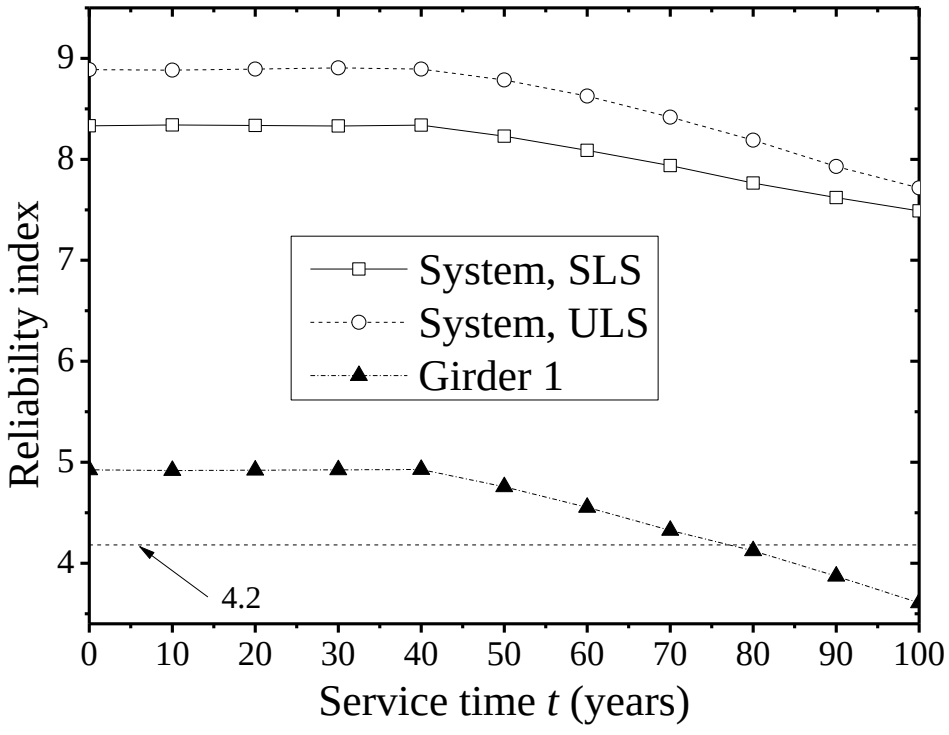

(b)

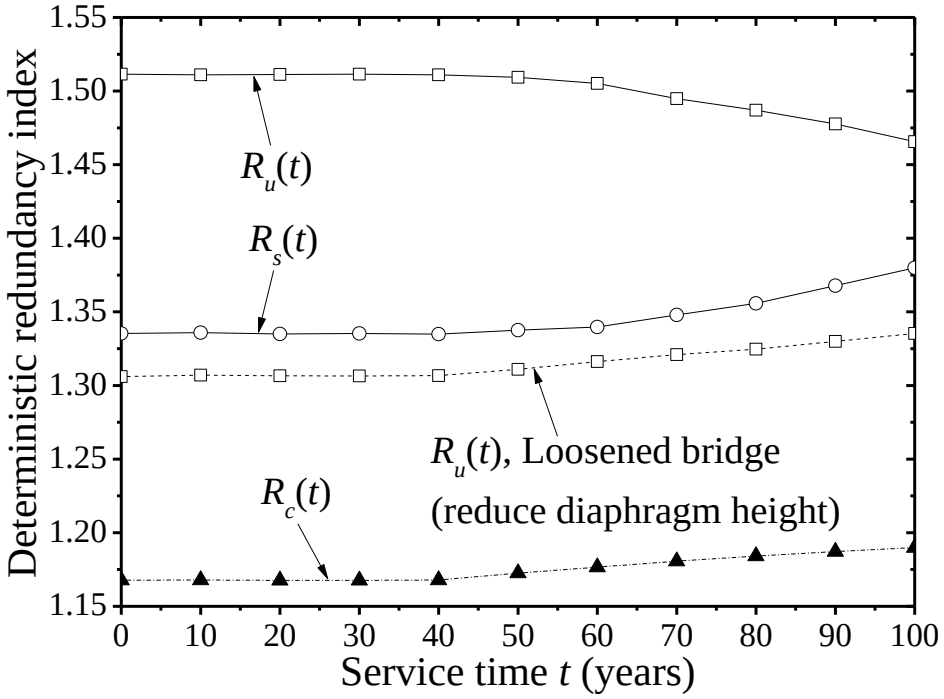

(a)

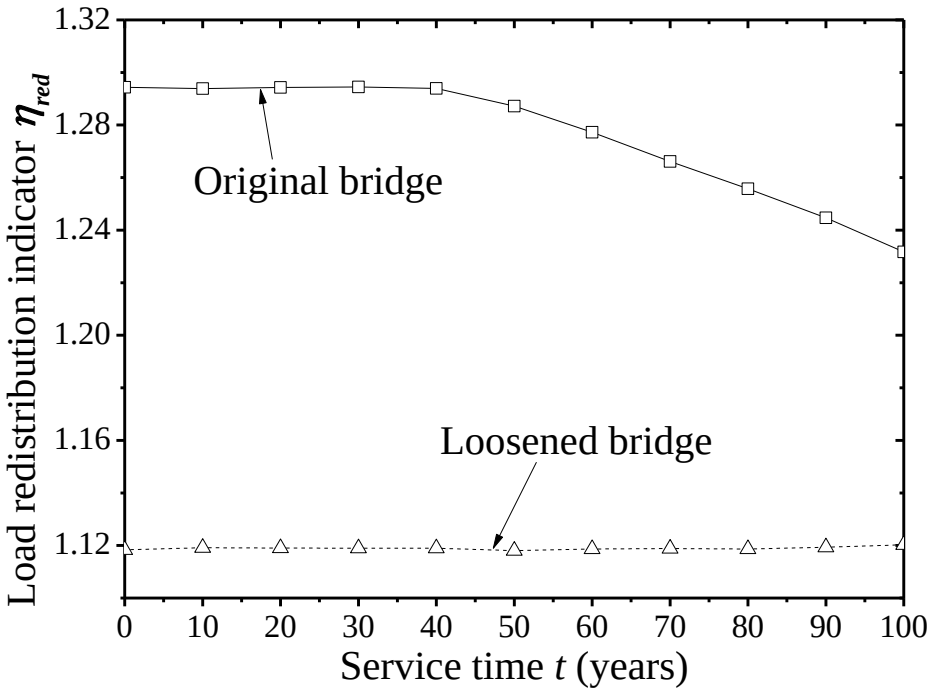

(b)

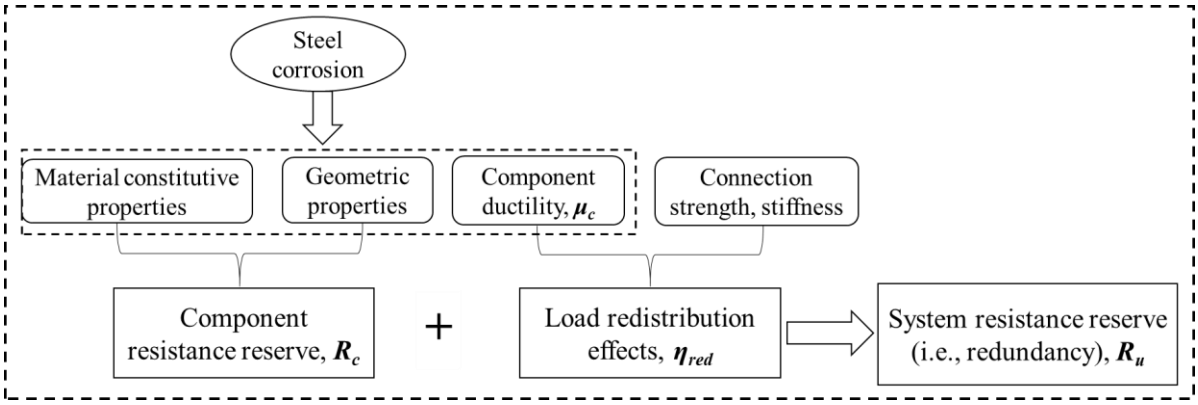

(a)

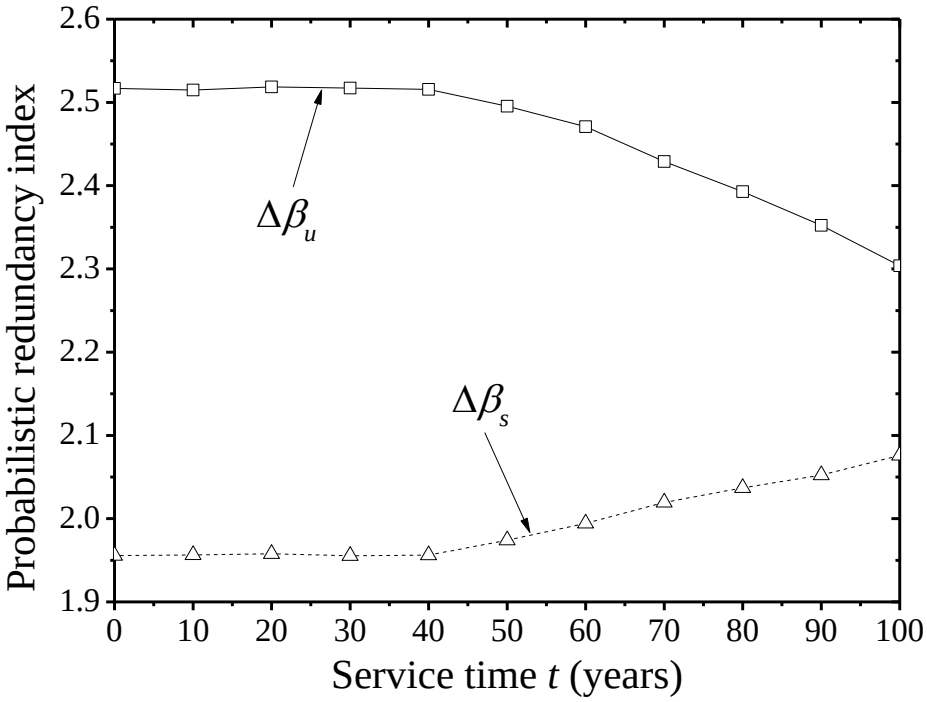

(b)

Figure Caption List